PCCP

RSC Publishing

PERSPECTIVE

View Article Online
View Journal | View Issue

Published on 01 November 2012. Downloaded by Universidade Federal do Parana on 22/05/2013 04:05:36.

Cite this: *Phys. Chem. Chem. Phys.*, 2013, **15**, 3027

What controls the composition and the structure of nanomaterials generated by laser ablation in liquid solution?†

Vincenzo Amendola* and Moreno Meneghetti

Received 18th August 2012,
Accepted 31st October 2012

DOI: 10.1039/c2cp42895d

www.rsc.org/pccp

Laser ablation synthesis in liquid solution (LASiS) is a ''green'' technique that gives access to the preparation of a library of nanomaterials. Bare noble metal spherical particles, multiphase core–shell oxides, metal–semiconductor heterostructures, layered organometallic compounds and other complex nanostructures can be obtained with the same experimental set up, just by varying a few synthetic parameters. How to govern such versatility is one of the current challenges of LASiS and requires a thorough understanding of the physical and chemical processes involved in the synthesis. In this perspective, the fundamental mechanisms of laser ablation in liquids are summarized, organized according to their temporal sequence and correlated with relevant examples taken from the library of nanomaterials disclosed by LASiS, in order to show how synthesis parameters influence the composition and the structure of products. The resulting framework suggests that, to date, much attention has been devoted to the physical aspects of laser–matter interaction and to the characterization of the final products of the synthesis. Conversely, the clarification of chemical processes active during LASiS deserves more research efforts and requires the synergy among multiple investigation techniques.

1. Introduction

In recent years, the laser ablation synthesis in liquid solution (LASiS) of nanomaterials (NMs) gained increasing interest for its versatility, low cost and ease of execution.[1] After the initial stage, in which the interest was focused on the characterization of synthesis products, now the number of scientific reports on LASiS of functional materials for specific nanotechnology applications is continually growing. For instance, NMs obtained by LASiS were applied in SERS labelling,[2,3] self-healing optical limiting devices,[4,5] friction-reducing coatings,[6] photonic materials,[7–11] antibacterial nanocomposites,[12] neural electrodes,[13] water splitting,[14] catalysis,[15] and cell sorting/targeting.[16,17]

In LASiS, the NMs are obtained by focusing laser pulses on a bulk target immersed in a liquid solution (Fig. 1).[1] The target can be either a single piece or pressed powder, although the dynamics of the synthetic process does not vary. Nanoparticles (NPs) formation may take place by various mechanisms like nucleation and growth or ejection of hot drops and solid fragments from the target.[18] The parameters of the synthesis are divided into two categories: material parameters (bulk target, solvent and solutes, system temperature and pressure)

Department of Chemical Sciences, University of Padova, Via Marzolo 1, I-35131 Padova, Italy. E-mail: vincenzo.amendola@unipd.it

† This article was submitted following the Laser Ablation and Nanoparticle Generation in Liquids (ANGEL 2012) Conference.

Vincenzo Amendola

Vincenzo Amendola (PhD in Materials Science and Engineering) is an Assistant Professor of Physical Chemistry at the University of Padova. He has been a visiting researcher at M.I.T. (Boston, US) and Cambridge University (Cambridge, UK). His research activity concerns laser assisted synthesis of multi-functional nanoparticles, plasmonics and self-healing nanomaterials.

Moreno Meneghetti

Moreno Meneghetti is a full professor of Physical Chemistry at the University of Padova. Among his research activities are synthesis and functionalization of metallic and carbon nanostructures and the modelling of their optical properties.

Published on 01 November 2012. Downloaded by Universidade Federal do Parana on 22/05/2013 04:05:36.

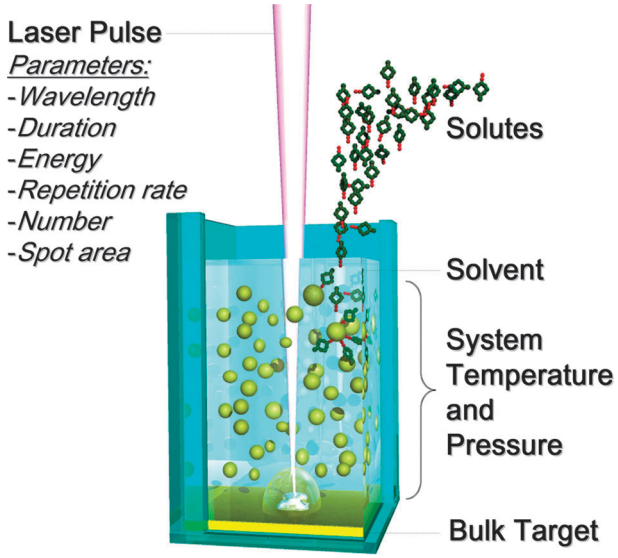

Fig. 1 Sketch of the main experimental parameters of LASiS.

and laser parameters (wavelength, duration, energy, repetition rate, number of laser pulses and the spot area on the target).[1]

In a different type of laser assisted synthesis, liquid dispersion of micro or nano particles is irradiated with laser pulses.[1] Laser irradiation is generally used to obtain the size refinement of nanomaterials, while maintaining their initial composition,[1,19–22] and it does not fall within the topic of this perspective.

Laser ablation induces physical modification of matter, due to the fragmentation from bulk into nanoparticulates. In most cases, chemical modification of matter occurs as well, *i.e.* the formation of new compounds and phases.[23,24] Therefore LASiS embodies some aspects of both physical top-down and chemical bottom-up synthetic methods.[1] This hybrid physical–chemical nature is reflected in the pros and cons of the technique. The main pros are:

- LASiS is a unique approach for the synthesis of a variety of nanomaterials in a variety of liquid solutions. A library of nanomaterials can be obtained by LASiS, with minimal variation in the process parameters (see Fig. 2). Indeed, there are companies providing customized NMs produced by LASiS on demand.

- LASiS is compatible with the 12 principles of "green chemistry", because it does not necessarily require chemicals and does not necessarily produce waste.[1] LASiS allows the development of sustainable nanotechnology, which is a prerequisite for crossing the boundary between research and everyday applied technology.[25]

- LASiS is a low-cost method because manual operation and the experimental set up are minimal, chemical precursors are replaced by bulk materials and other expensive chemicals are seldom used. These features also facilitate the batch-to-batch and the lab-to-lab reproducibility of the synthesis and the biocompatibility of the products.

- In several cases, inorganic nanoparticles coated with organic molecules can be obtained in one step, *in situ* (*e.g.* during the synthesis) or *ex situ* (*e.g.* after the synthesis).[1]

- LASiS is one of the fastest, cheapest and cleanest ways to produce colloidal NMs with size dispersion below 100 nm on the milligram scale.[26]

The cons of LASiS are the following:

- Although gram scale production has been recently reported,[26] such productivity is still far from that achieved by other methods like spray pyrolysis or wet chemistry synthesis.

- The control of NMs size distribution is usually lower than that by state of the art wet chemistry methods.[22,27]

- The control of NMs shape is not possible, except for a few cases.[28]

- Heterogeneous synthetic parameters are observed in the scientific literature and the comparison of results from different groups is sometimes difficult. Indeed, every lab equipped with a pulsed laser can produce its own NMs, and LASiS is a young technique still under development, for which there are no universally defined procedures.

Additional pros and cons should be considered for each specific NM in the library accessible by LASiS. For instance, gold

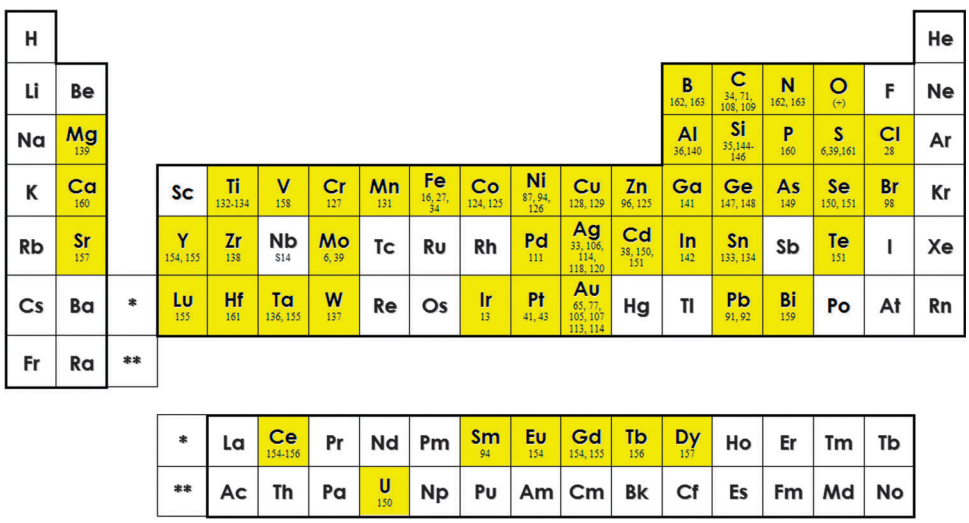

Fig. 2 The library of NMs available for LASiS is summarized in the periodic table. Yellow entries indicate the main elements of the compounds obtained by LASiS. Some representative references are provided below each element. (+): for the references of oxygen see Section 3.

 This journal is © the Owner Societies 2013

Published on 01 November 2012. Downloaded by Universidade Federal do Parana on 22/05/2013 04:05:36.

nanoparticles (AuNPs) obtained by LASiS can be functionalized with multiple molecules,[29] and sensing of surface coating is possible by optical absorption spectroscopy.[22,30,31] Nanocomposite materials or doped wide band gap semiconductor nanoparticles can be obtained in one step.[14,32,33] NPs of transition metals and semiconductors can be obtained, which are stable in air by formation of a passivating layer.[34–36] Ferrimagnetic iron oxide phases can be preferentially obtained instead of antiferromagnetic ones.[16,27] Metastable phases can be found among the laser ablation products.[37] On the other hand, the composition of the target is not necessarily found in the final NMs because of side reactions with the liquid solution.[13,38] Especially with alloy targets, NPs stoichiometry can be very different from that of the bulk target.[13] Frequently, a mixture of products with heterogeneous phase, structure and morphology is obtained.[39]

In principle, the yield of desired products can be maximized by the choice of appropriate experimental parameters, once the connection between the two aspects is known. Therefore, the ability to control the phase and the structure of NMs requires a thorough understanding of the physical and chemical processes involved in LASiS. Such an ambitious goal can be pursued only by multidisciplinary investigation skills, which are seldom gathered by a single research group active in the field. Moreover, as recalled above, the variety of experimental conditions reported in the literature makes it difficult to extrapolate a comprehensive picture of the problem. Consequently, there are many unclear points about the correlation between experimental parameters of LASiS and the formation of NMs.

In this perspective, we afford the problem by dividing it into two parts. In the first part, the fundamental mechanisms of LASiS are sketched, paying attention to the temporal sequence of the processes and recalling the investigation techniques used so far.

In the second part, we selected some relevant examples from the library of NMs attainable by LASiS, and we used them to show how the variation in experimental parameters yields significant modifications of the products. We frequently start the discussion by referring to the simple case of a generally inert material like gold and then moving towards more reactive compounds, like silver and iron, which give different products upon minimal changes in synthetic conditions.

The discussion can help in guiding towards the LASiS of NMs with the desired phase and composition. Besides, several points that deserve particular attention are highlighted like the chemical reactions occurring in LASiS and the spatio-temporal evolution of temperature, of pressure, of the concentration of ablated species and of the concentration of solution species. Shedding light on such aspects is a complicated task which needs complementary physical–chemical skills, but it is a mandatory step to control and expand the library of NMs disclosed by LASiS.

2. Basic mechanism of LASiS

The main stages of LASiS can be resumed as follows (see Fig. 3): the process starts with the absorption of the laser pulse by the bulk target, then a plasma plume containing the ablated material expands into the surrounding liquid, accompanied by the emission of a shockwave. During the expansion, the plasma plume cools down and releases energy to the liquid solution. This phenomenon generates a cavitation bubble which expands in the liquid and then collapses on a time scale of the order of hundreds of microseconds, by emission of a second shockwave.

We can identify 4 main parameters whose profiles in time and space primarily determine the phase and structure of final NMs: temperature (T), pressure (P), concentration of the ablated material (C_M) and concentration of solution species (C_S). The most complex point in LASiS is that, due to the hemispherical symmetry of the laser ablation phenomena, the 4 parameters are not uniform in space neither constant in time. To gain a better perspective on the evolution of the 4 parameters, it is instructive to describe the temporal sequence of the ablation stages when a single laser pulse hits the target (Fig. 4). In the following, we assume that the fluence is above the ablation threshold (usually in the 10–10^3 J cm^{-2} range) and we set the time $t = 0$ as the instant when the laser pulse hits the target.

2.1 Temporal evolution of physical–chemical phenomena in LASiS

For $t < 0$: pulse penetration in the liquid. The laser pulse must pass through a layer of liquid before reaching the target. Laser energy should be delivered to the target only, and not to the liquid solution. In particular, liquid breakdown must be avoided.[40–42] With a pulse duration (τ_{pulse}) of picoseconds (ps) or longer, breakdown is avoided by working under defocused conditions. With τ_{pulse} of femtoseconds (fs), relevant nonlinear optical effects like self-focusing are observed at fluences required for laser ablation, therefore also the thickness of the liquid layer must be reduced to maintain the defocusing conditions.[42] In all cases, there is a fluence threshold (F_{th}) that must not be exceeded in order to avoid nonlinear optical effects like multiphoton absorptions from the liquid.[43] Fixed the energy per pulse, longer pulses have higher F_{th} and permit the delivery of more energy to the target.

The liquid solution should be transparent at the laser wavelength, although there are frequent exceptions to this rule. For

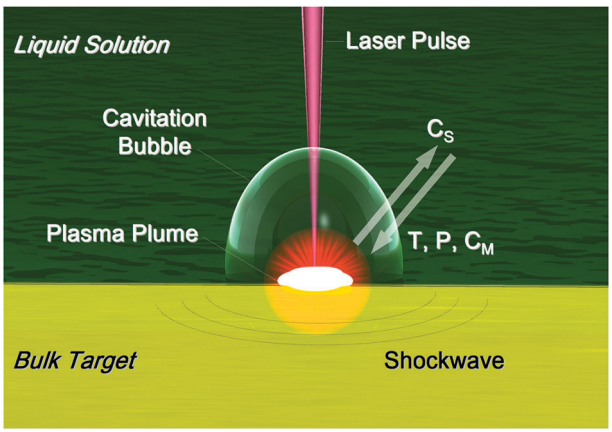

Fig. 3 Sketch of the main stages of LASiS (for details, see the text). The white arrows indicate that, upon increasing the distance from the laser spot, the temperature (T), pressure (P) and concentration of the ablated material (C_M) decrease, while the concentration of solution species (C_S) increases.

Published on 01 November 2012. Downloaded by Universidade Federal do Parana on 22/05/2013 04:05:36.

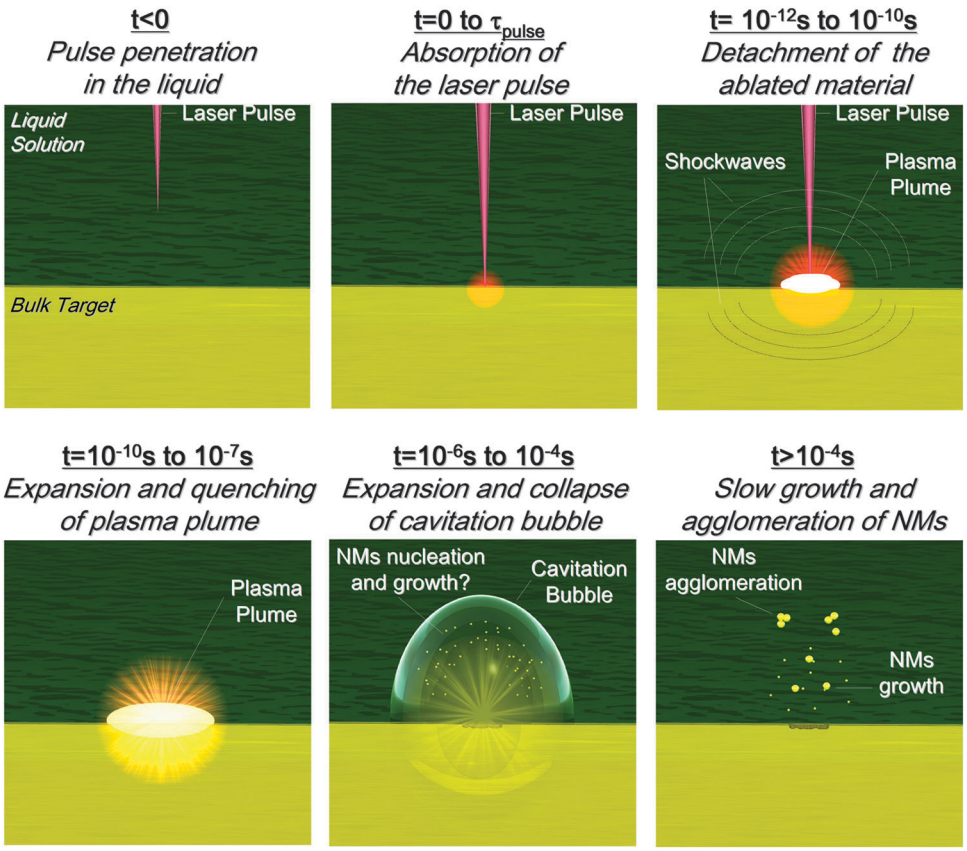

Fig. 4 Sketch of the timeline of LASiS. Ablation with ns pulses has been considered in this example. Nucleation and growth of NMs are hypothesized in the 10^{-6}–10^{-4} s time range, although precise information is lacking. For details see the text.

instance, water absorption at 1064 nm is not null. Usually, under ordinary LASiS conditions, it is assumed that solvent absorption does not play a relevant role in NPs formation, because the portion of energy delivered to the target is orders of magnitude larger than that absorbed by the liquid. Only in specific cases the liquid solution can significantly absorb or scatter laser light, due to the presence of absorbing solutes or of already formed NPs, with consequent reduction of the energy transferred to the target.

From t = 0 s to τ_{pulse}: absorption of the laser pulse. Due to the high photon density, linear and nonlinear absorption processes occur when the laser pulse hits the target.[44–46] The thickness of the target in which light is absorbed is of the order of the material skin depth.[45] Nonlinear optical processes depend on the electromagnetic field intensity, which is proportional to the pulse fluence f divided by the pulse duration τ_{pulse}.[45]

At the fluence required for LASiS, pulses of less than a few ps lead preferentially to instantaneous multiphoton absorption processes and, on cascade, to localized photoinduced ionization.[45,47] Since optical absorption is simultaneous to laser–matter interaction, direct photoionization lasts for a time equal to τ_{pulse}.[47]

Direct photoionization is highly probable for a pulse duration of up to 10^{-8} s.[47] However, by increasing τ_{pulse} above 10^{-12} s, that is the minimum time required for the electron–lattice thermalization,[48,49] the electron kinetic energy can be released as thermal energy to the lattice.[50] In this case, thermal processes like thermionic emission, vaporization, boiling and melting may occur simultaneously to photoionization, affecting a larger volume than that defined by the spot area and the target skin depth.[23,50,51]

For $t = 10^{-12}$ s to 10^{-10} s: detachment of the ablated material. After multiphoton absorption and direct photoionization, the locally induced space-charge separation fields and electron–ion collisions initiate, on a timescale of 10^{-12} s, the detachment of matter from the target.[45,48,49] Then, the detachment proceeds sustained also by the transfer of kinetic (thermal) energy from excited electrons to the lattice, namely by heating of the lattice, which occurs on a timescale of several ps.[45,48,49]

The temperature difference between the irradiated zone and the rest of the system is very large, and solid targets dissipate heat very efficiently, therefore material detachment occurs by thermal and coulombic mechanisms in a region almost coincident with the laser spot.[42,45,47,52]

In the literature, no differences were reported in the detachment of ablated material, on the timescale of 10^{-12} s to 10^{-10} s, when the process takes place in gas or in liquid phase.[42,45,47,52] However, physical parameters of detached material are crucial for following steps of NMs formation (nucleation, growth and reactivity with solution species). Therefore, understanding the process of material detachment is a key point for controlling the versatility of LASiS.

The precise description of the ablation mechanism is not simple and multiple fragmentation processes are possible, depending on laser parameters, even simultaneously in different locations within the laser spot.[23,48,49] The most popular theory exploits classical

 This journal is © the Owner Societies 2013

Published on 01 November 2012. Downloaded by Universidade Federal do Parana on 22/05/2013 04:05:36.

thermodynamics as a first approximation to describe laser ablation.[46] In this frame, only three kinds of thermal processes may lead to material detachment from a laser-irradiated target: vaporization, normal boiling and "explosive boiling".[46] Under ordinary LASiS conditions and with laser pulses shorter than 10^{-7} s, "explosive boiling" is considered the main thermodynamic mechanism of material detachment from the crater.[46,48,49,53] Explosive boiling, also called "phase explosion", occurs when solid matter is rapidly superheated up to the thermodynamic critical temperature, at which the spinodal decomposition in vapor and liquid phase in the irradiated material occurs by homogeneous nucleation.[46]

When energy is transferred to the target by ps and fs pulses, however, molecular dynamics calculations evidenced that material detachment is too fast and far from thermodynamic equilibrium to be described by explosive boiling.[48,49,53,54] In this case, the ablation mechanism is generically defined as "fragmentation" and consists of the detachment of hot atoms, vapors and liquid drops under out of equilibrium conditions (Fig. 5).[54]

The temperature–density phase diagram with typical paths yielding different mechanisms of material detachment from a target is shown in Fig. 6.[53] Pulse energy and duration determine different heating rates, which in turn correspond to different paths in the diagram.[23,48,49,52–54]

It is worth defining first the difference between slow and fast heating in laser ablation: slow heating means that energy is released on a time scale much longer than the electron–phonon relaxation time (of the order of 10^{-12} s), while a fast heating process occurs on a time scale of less than 10^{-12} s. Therefore, the pulse energy defines the maximum temperature reached by the target and, for a given pulse energy, vertical segments in the diagram correspond to ablation with ultrafast laser pulses (10^{-12} s or less), while curved segments are possible with pulses longer than about 10^{-12} s.

In the case of slow heating (*i.e.* ms and μs pulses), the system follows the binodal curve (path A → B), where gas and liquid coexist in equilibrium, then material detachment occurs by vaporization and boiling.

For shorter pulses (*i.e.* pulse duration of *ca.* 10^{-8}–10^{-10} s), the heating and concomitant density drop drive the system in the region of spinodal decomposition (path A → C), where the explosive boiling occurs. By further reducing the pulse duration (*i.e.* ps pulses) or increasing the pulse energy, the system can be driven directly to the gas region without crossing the binodal curve (path A → D), then the fragmentation takes place. For ultrashort pulses (*i.e.* fs pulses) at high fluence, energy is transferred to the material on a time scale so fast that no density variation can occur simultaneously to heating, therefore the process starts with a vertical line (isochoric heating). Depending on the amount of energy released in the material, the expansion and cooling can lead either to the spinodal region by adiabatic cooling (path A → E) or to the gas region by direct fragmentation (A → F).

Although thermodynamics and MD provide useful information about the first instants of material detachment from the target, several obscure points are principally related to the effect of photoionization, of photomechanical stress and of plasma confinement on the crater surface due to the liquid buffer. In particular, photoionization could contribute to material detachment by coulombic explosion,[47] similar to what was observed during laser irradiation of particle suspensions.[55]

Simultaneously to the ablation process, the recoil pressure of the ablated material drives one shockwave propagating into the target and a second specular shockwave counterpropagating into the liquid solution, with supersonic velocity (of the order of 10^3 m s^{-1}).[44,56] A shockwave is a pressure wave travelling in a medium and implies an abrupt discontinuity in density and temperature along its front.[56]

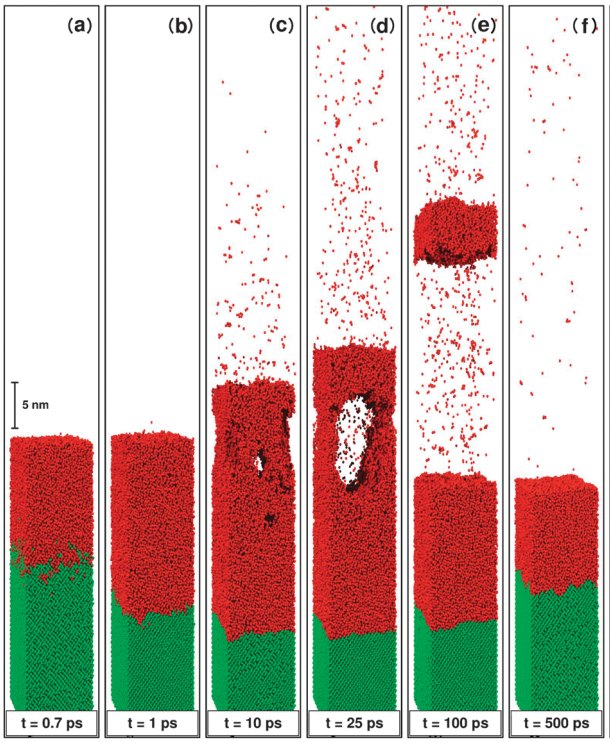

Fig. 5 Snapshots of solid "fragmentation" calculated by molecular dynamics simulations, which show the structural evolution of the Si(100) substrate irradiated with a 500 fs (266 nm) laser pulse at a fluence of 0.255 J cm^{-2}. Green: solid semiconducting Si; red: liquid metallic Si. Reprinted with permission from ref. 54.

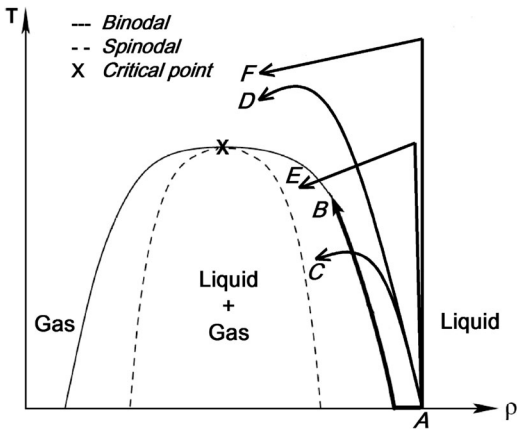

Fig. 6 The typical paths yielding different mechanisms of material detachment from a target are reported in the temperature (T)–density (ρ) phase diagram. Curved trajectories (A, B, C, D) are possible only by slow heating (pulse duration longer than 10^{-12} s), while vertical lines (E, F) are possible only with ultrafast heating (pulse duration shorter than 10^{-12} s).

Published on 01 November 2012. Downloaded by Universidade Federal do Parana on 22/05/2013 04:05:36.

The energy of shockwaves generated by laser ablation is of the order of 10–50% of the absorbed pulse energy.[57] Shockwave propagation heats the liquid and the target and may promote the detachment of matter from the crater.[32,58,59]

The ablated material contains highly ionized species due to high temperature and direct photoionization, hence it is considered a non-equilibrium "plasma plume".[44] The plasma plume generates light with an emission spectrum composed of continuous background and discrete lines.[60,61] The continuous emission background is caused by bremsstrahlung and radiative recombination, while discrete emission is typical of the relaxation of excited atomic and molecular species.[44,60,61] Plasma temperature, pressure and density are of the order of 10^3 K, 10^{10}–10^9 Pa and 10^{22-23} atoms per cm^3 respectively.[26,44,60,61] After the end of the laser pulse, the plasma plume has a lifetime of the order of tens of ns: in the first ns, the emission is dominated by the continuum, while discrete atomic and molecular lines prevail in the last ns.[60,61] The evolution kinetic of the plasma plume is very fast, because heating by the laser pulse abruptly alternates with cooling due to plume expansion and heat exchange with the solvent. Moreover, melted drops and, sometimes, solid fragments can be present in the plasma plume.[62,63] Therefore, thermodynamic equilibrium is not reached in the plasma plume and its emission does not obey Planck's law.[60,61]

When τ_{pulse} is of the order of 10^{-11} s or more, there is a temporal and spatial overlap of the laser pulse with the plasma plume, meaning that the plume itself can absorb energy from the laser pulse.[64] This effect is called "plasma shielding" because it reduces the amount of laser energy directly delivered to the target, while increasing the temperature and the lifetime of the plasma plume.[45,63]

For $t = 10^{-10}$ s to 10^{-7} s: expansion and quenching of plasma plume. Although in the first picoseconds after the arrival of laser pulse, the physics is similar for laser ablation in gas or in liquid, for $t = 10^{-10}$–10^{-9} s an important difference is observed because the liquid buffer strongly confines the plasma plume onto the crater area.[49,56] The confinement slows down the cooling rate at the interface between the ablated material and the target, because the hot ablated material can provide thermal energy to the underlying target. As a final result, the ablation yield in liquid is higher than in gas because a larger portion of the target reaches the energy threshold for detachment.[59–61,64] The important result is that, in liquid, target ablation takes place by energy transfer both from the laser pulse to the solid target and from the plasma plume to the heated target, and the latter process may prosecute for several nanoseconds after the end of the laser pulse.[59–61,64,65]

For times shorter than about 10^{-10} s, the spatial gradients of T, P, C_M and C_S can be considered very sharp and one can identify three regions: the solid target, the expanding plasma plume and the liquid solution.[48,49,53,54] After about 10^{-10} s, the plasma plume expands and cools in the solution by releasing its energy to the liquid buffer on one side, and to the solid target on the other side. The liquid is heated up to temperatures of the plasma plume, *i.e.* 10^3 K, with consequent degradation, ionization and pyrolysis of solution molecules.[60,61] During this process, the spatial gradients of T, P, C_M and C_S become smoother and rapidly change in time and space, while target and solvent species mix together.[60,61] Semiquantitative estimations of these gradients are accessible by experimental and theoretical studies, but their reliable quantitative evaluation is missing at the moment.

A very important point of LASiS is the lack of clear information about the timescale of the nucleation and growth processes. The time at which nucleation starts strongly depends on concentration, temperature and pressure and, therefore, it cannot be inferred by the literature concerning laser ablation in gas. Some authors suggested that nucleation starts after only about 10^{-9} s,[37] while others more realistically suggested longer times up to 10^{-5} s.[18,64] However, reliable experimental evidence is missing and, in particular, it is not clear if the nucleation and growth of nanoparticles take place before or after extensive mixing of ablated and solution species and what is the ionization state of solution species when it happens. Optical emission spectroscopy confirmed that reactions between target and solvent species may occur already in the plasma plume,[60,61] but did not provide quantitative information about the relevance of such a phenomenon.

The fate of melted drops ejected from the target also deserves further investigation. For instance, it is not clear if molten material preferentially undergoes solidification or further vaporization and, subsequently, NMs nucleate and grow. Besides, during laser ablation in gas, a fraction of the detached material is redeposited into the crater, while it is not clear what is the extent and what are the parameters governing this process during laser ablation in liquids.[66] It should be considered that liquid drops, solid fragments and molecular clusters compose the ablated material[62] and may act as preferential sites of growth and coalescence. In this case, the nucleation stage may be not important in LASiS, because nuclei are directly extracted from the target simultaneously to the ablation process. In order to clarify this point, a deeper understanding of the target fragmentation mechanism would be required.

NMs obtained by laser ablation are prevalently polycrystalline, meaning that nuclei coalescence must take place.[1] NPs usually have spherical shape, therefore nuclei coalescence happens when the interface energy can be minimized by lattice rearrangement. It means that, during coalescence, the nuclei are melted or, at least, their temperature is high enough to allow the mobility of interface atoms. Free atoms adsorbed from the solution may also play a role in smoothing grain interfaces, if the process occurs when NPs are still hot. Therefore, LASiS generates NMs by a hybrid mechanism between top down physical methods and bottom up chemical methods. In top down physical methods, bulk matter is fragmented down to nanometric size without going through the atomization of matter and, ideally, it yields monocrystalline NMs when the bulk is a monocrystal.[67] In bottom up chemical methods, nucleation is frequently followed by a stage of slow growth fed by atomic precursors, while nuclei coalescence is hampered by a layer of stabilizers.[67] The same layer can act as a template for obtaining anisotropic shapes by directing the growth along selected crystallographic directions.[67] In LASiS, it is likely that a mixture of clusters and atomic precursors is generated by laser ablation under conditions of supersaturation, namely the vapour pressure of ablated species is larger than their equilibrium vapour pressure at room temperature, hence nucleation and/or growth rapidly occur.[1] The formation of anisotropic shapes by adding molecular templates is

 This journal is © the Owner Societies 2013

Published on 01 November 2012. Downloaded by Universidade Federal do Parana on 22/05/2013 04:05:36.

not effective with LASiS due to the fast kinetics of formation, unless the ablated atomic precursors are stabilized by the solution.

The size distribution of NPs obtained by LASiS is always lognormal.[1] The sole exception is when laser pulses modify already formed NPs. Granqvist *et al.* showed that NPs have lognormal size distribution when their growth is fed by atom diffusion simultaneously to the drift of NPs through a finite growth region.[68,69] Subsequent NPs agglomeration does not influence the lognormality if it takes place under the same drift conditions.[68,69] In LASiS, the finite growth region is the area between the target and the liquid solution, while NPs drift velocity is provided by the expansion of the ablated material.

For $t = 10^{-6}$ s to 10^{-4} s: expansion and collapse of cavitation bubble. The plasma plume is typically extinguished after a time of 10^{-8}–10^{-7} s.[70] The energy released by the plasma plume to the surrounding liquid induces the rise of a cavitation bubble on a timescale of 10^{-7}–10^{-6} s, which expands up to times of the order of 10^{-4} s (Fig. 7).[64,70] The bubble travels with supersonic speed (>10^3 m s^{-1}) in the liquid up to a maximum radius of the order of millimeters, under ordinary LASiS conditions.[64,70,71] During its expansion, bubble's temperature decreases and bubble's internal pressure drops to a value lower than in the surrounding liquid. At this stage, the bubble collapses emitting a shockwave.[70,71] This is the last physical process related to laser ablation of a target in liquid solution.

It is not clear what is the stage of NPs formation and their spatial distribution when the expansion of the bubble starts or ends. In principle, already formed NPs can travel in front of expanding cavitation bubbles.[72] However, some authors suggested that NMs are formed inside the bubble during its expansion, on a time scale of 10^{-6}–10^{-4} s.[18,52,59,64] Since the NMs come from the initially hot plasma region, and the cavitation bubble originates by the release of heat from this region to the surrounding liquid, the hypothesis that NMs are inside the bubble is realistic. This is a relevant point because the concentration of solution species inside the bubble is much lower than in the liquid. In addition, solution species inside the bubble are in higher energetic states and also the temperature inside the bubble is higher than in the surrounding liquid during bubble expansion. Thermal conductivity of the gas is lower than that of the liquid, therefore NPs that form inside the bubble remain hot for longer time than in the liquid.[59,64] For the same reason, the temperature gradient at the bubble/liquid interface may promote nucleation and condensation of NMs.[73] There is experimental evidence that excited target species still exist inside the cavitation bubble, but there is no quantitative insight into the spatial distribution of the ablated matter, namely one cannot exclude that the majority of NMs are already formed and are located elsewhere in the solution.

When the bubble collapses, high energy is released by emission of a shockwave.[74] It has been evaluated that temperature and pressure of the same order of the plasma plume (10^3 K and 10^{10} Pa) are reached in the collapse point, with possible effects like aggregation and phase transition of the already formed NMs or material detachment from the target.[32,70]

For $t > 10^{-4}$ s: slow growth and agglomeration of NMs. After the shockwave generated by the collapse of the cavitation bubble, the system reaches steady state physical and chemical conditions. In this stage, NMs can undergo minimal modifications due to the condensation of ablated atoms and molecular clusters that still survive in solution.[75,76] If NMs dispersion is not stable, agglomeration starts, which will yield precipitation on a timescale longer than minutes for micrometric and nanometric particles.[77] Depending on the NPs composition, also surface oxidation can occur or prosecute at this stage.

2.2 Investigation techniques

The direct investigation of laser ablation in liquid buffers is very challenging for the following reasons:

- most structural investigation techniques do not possess the time resolution required for tracking the ultrafast dynamics of LASiS;
- the spatial resolution required for accurate investigation of the ablation process exceeds that of most conventional techniques;
- the geometry of the problem is hemispherical, with multiple concentric layers corresponding to different physical conditions, and each layer shields the inner ones;
- the amount of material to be investigated is of the order of 10^{-1}–10^{-3} μg per pulse,[1] which is below the limit of sensitivity of most structural investigation techniques;
- light emission from the plasma plume and the laser pulse itself interferes with most optical absorption spectroscopic techniques.
- Mass spectrometry techniques cannot be implemented in the LASiS configuration.

So far, the following techniques have been used for the investigation of the laser ablation process and real time nanoparticles formation (Fig. 8):

Time resolved optical emission spectroscopy was used for plasma diagnostics with sub-ns time resolution and sub-millimetric spatial resolution (if carried out with a CCD camera).[60,61,70,78] The sensitivity of emissive species like single atoms and small molecules can reach the ppm range under best conditions.[70] The chance to perform

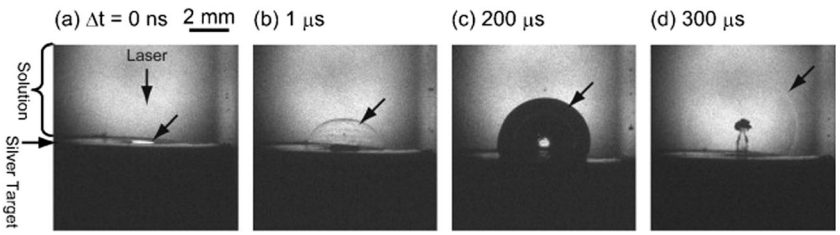

Fig. 7 Snapshots showing the evolution of the cavitation bubble during laser ablation of an Ag target in aqueous solution. From left to right: (a) light emission from the plasma plume, (b) first shockwave, (c) rise of the cavitation bubble, (d) collapse and generation of the second shockwave. Reprinted with permission from ref. 64.

Published on 01 November 2012. Downloaded by Universidade Federal do Parana on 22/05/2013 04:05:36.

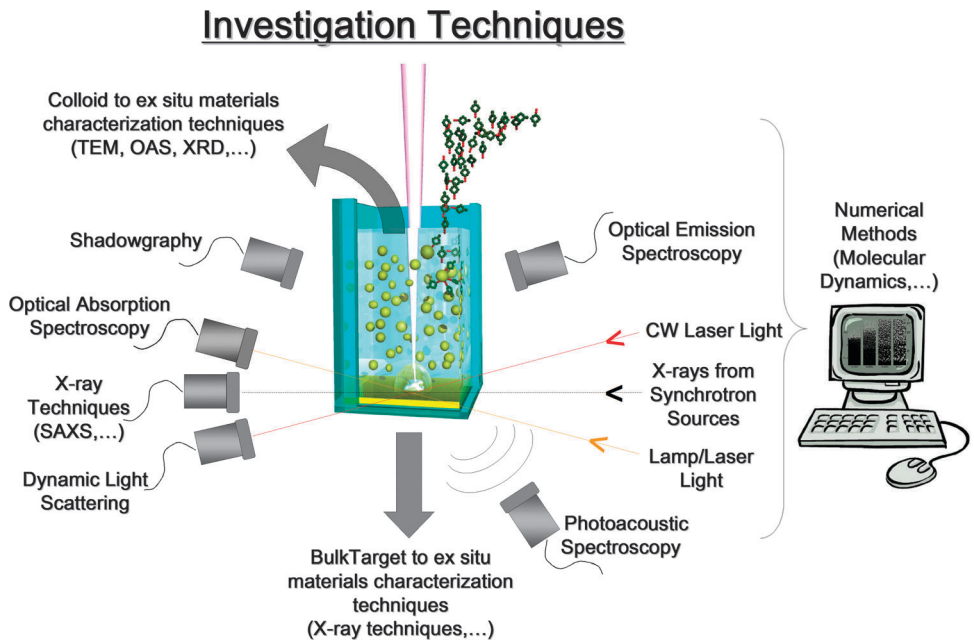

Fig. 8 Sketch of the techniques used so far for the investigation of LASiS. For details see the text.

double pulse laser induced breakdown, though not frequent in LASiS, may theoretically provide quantitative information about the concentration of ablated and solution atomic species.[60,61,70]

Time resolved ns-shadowgraphy provides information on the time evolution of the plasma plume, of the shockwaves and of the cavitation bubbles with a micrometric spatial resolution.[59,64,79,80]

Photoacoustic spectroscopy can be performed with a time resolution of the order of 10^{-6} s and provides information on the time evolution of shockwaves.[64,81]

Optical absorption spectroscopy can be performed with sub ns time resolution and with millimeter spatial resolution by using a CCD streak camera.[80,82] To date, pump and probe optical spectroscopy was not exploited for LASiS, maybe due to the interference of continuum light emission from the plasma plume.

Dynamic light scattering provides information on the presence of objects with a size of a few nm or larger, with a time resolution of minutes. The technique does not discriminate between bubbles and NPs and signals are strongly dominated by larger objects. The spatial resolution is of the order of 10^{-3} m, which is the spot of the cw laser used in this technique.[80,82]

Very recently, time resolved X-ray techniques have been applied for real time investigation of NMs formation during laser ablation.[83] The great advantage of X-ray techniques is the selectivity for condensed phases and high atomic weight materials. However, these methods require ultrabright time resolved X-ray sources like synchrotron radiation in order to get detectable signals with time resolution of the order of ns or μs. Various X-ray techniques are ideally exploitable and available from the synchrotron source, like wide angle scattering (X-ray diffraction – XRD), small angle scattering (SAXS), absorption (XAS and all its variants). As the first step, the attention has been concentrated mainly on SAXS, probably because it gives relatively intense signals, provides information on the size of NMs instead of their composition (in contrast to XAS) and was already exploited successfully for the investigation of laser photofragmentation of NPs.[84,85]

Most of the above techniques produce volume weighted signals, namely a single micrometric fragment detached from the target produces more signal than thousands of nanometric nanoparticles. Given the size polydispersity of NMs obtained by LASiS, this is another severe limitation for the investigation of the mechanisms of laser ablation.

Theoretical and numerical models can ideally overcome most limitations of the experimental investigation techniques. Laser ablation and NPs formation can be modelled with atomic spatial resolution and virtually unlimited temporal resolution by molecular dynamics (MD).[23,48,49,53,54,62]

The non-thermodynamic equilibrium conditions of laser ablation are well reproduced by MD calculations, usually treating the cascade of electron–ion collisional events with a Monte Carlo approach.[54] One of the drawbacks of MD calculations performed so far is that they do not account for ultrafast nonlinear optical phenomena, like photoionization or multiphoton absorptions, for space-charge separation fields and for coulomb explosion.[23,48,49,53,54,62] Moreover, the unit cell of the model is limited to a small portion of the target, which is an acceptable approximation for modelling the ablation process, but is less reliable for modelling the NMs nucleation and growth process and the interaction with solution species.

3. Effect of LASiS parameters on composition and structure of NMs

The main, obvious, parameter of LASiS is the target material. However, due to a complex cascade of physical–chemical phenomena, laser ablation in liquids does not necessarily give NPs with the same phase and composition of the bulk target. Moreover, different

 This journal is © the Owner Societies 2013

Published on 01 November 2012. Downloaded by Universidade Federal do Parana on 22/05/2013 04:05:36.

materials show different reactivity and yield different products under the same experimental conditions. In general, all the materials and laser parameters of LASiS affect the final NMs. In the following sections, we discuss this topic one parameter at time. Since gold is an inert material and the LASiS of AuNPs was investigated intensively in past years, we frequently refer to the case of Au, and then we eventually consider the examples of more reactive materials taken from the recent literature.

3.1 Laser parameters

Pulse wavelength. The overlap of already formed NPs with incoming laser pulses occurs in the most ordinary LASiS set up, therefore the use of wavelengths that are not absorbed by the NMs is preferred to avoid interaction with the products. If NPs absorb laser pulses, they may undergo further modifications during the synthesis.[1,86,87] For instance, in LASiS of AuNPs with 532 nm or 355 nm pulses, photofragmentation takes place simultaneously to laser ablation.[1] The typical outcomes are the broadening of the size distribution and the decrease in average size.[1,86,87] Photoinduced heating of NPs can also promote the reaction with other species in solution and the degradation of nearby organic molecules.[88]

The skin depth (*i.e.* the absorption coefficient) of the target depends on pulse wavelength. Usually, at shorter wavelengths, the absorption coefficients of solid materials are larger. For instance, UV radiation is efficiently and uniformly absorbed by interband transitions in metal targets, yielding the regular erosion of all the irradiated area.[52] Conversely, near infrared radiation is absorbed preferentially by defects and impurities in the metal target, generating a rugged erosion profile on the spot area.[52,89] Also multiphoton absorption and photoionization processes are favoured at short wavelengths, with consequences on temperature, pressure and ionization state of the plasma plume.[23] More reactive species are formed by UV laser ablation, and chemical reactions between target and solution species that are not observed with NIR pulses may happen with UV pulses, as discussed later in the section on ''Solutes''.

UV and NIR wavelengths are considered to be two opposed extreme cases, while visible light shows intermediate properties.[52]

Pulse energy. The pulse energy affects the amount of ablated material and the ablation mechanism.[23] NPs productivity increases almost linearly with pulse energy as far as the dominating ablation mechanism remains the same.[42,76,86] This is the case, for instance, of LASiS of AuNPs with 1064 nm and ns pulses in the 10–100 mJ per pulse range (with spot size of the order of 10^{-3} m).[75] When the pulse energy is increased, larger size distributions and larger average NPs size are observed.[43] This is the concomitant effect of the larger amount of ablated material, which implies an higher concentration of target species in the plume, and of the detachment of solid and melted fragments, which is more probable at high energy.[23] More in detail, by increasing the pulse energy, multiple mechanisms of material detachment are simultaneously possible, like fragmentation, phase explosion, boiling and vaporization.[23,42,49,52] However, thermal mechanisms are more probable on the edge of the crater, while fragmentation is more probable in the central part of the laser spot.[23,42,49,52] For instance, AuNPs with a bimodal size distribution are obtained by fs LASiS at high energy, due to the coexistence of multiple ablation mechanisms, while a monomodal size distribution is achieved at low energy.[42,90] Similar results have been reported for ns LASiS of PtNPs.[43]

Pulse duration. Pulse duration (τ_L) has a strong influence on NMs size distribution, structure and composition. By using the same fluence but increasing τ_L, thermal mechanisms of ablation are favoured at the expense of photoionization mechanisms, as discussed in Section 2.1.[23,48,49,53,54]

The crater left by the laser pulse on the target shows very well the occurrence of thermal ablation processes, either in gas[45] or in liquid phase.[42,65] With fs pulses (Fig. 9A), the crater has sharp borders and matches the laser spot, which is typical of ultrafast localized heating (see paths A–F and A–E in Fig. 6) and of ablation dominated by direct photoionization processes and consequent locally induced space-charge separation fields and electron–ion collisions.[23,45] With pulses of tens of ps or longer, the craters are less sharp (Fig. 9B and C), which is typical of the coexistence of direct photoionization and thermal ablation processes like vaporization, boiling and ejection of melted material due to the high pressure generated in the crater.[23,52] This is because pulse duration is comparable to the electron–lattice thermalization speed, and the conduction of heat outside the laser spot can happen while the source of energy (the laser pulse) is still present.[45,63]

With ns pulses, the ablated material and the laser pulse coexist for a relatively long time due to plasma shielding.[45,63] This time is enough to transfer part of the laser energy to the plasma plume, with a consequent increase in its temperature, pressure and lifetime.[45,63] Under such conditions, the melted drops ejected from the target into the plume have higher chance to be further vaporized. Indeed, very large (>50 nm) AuNPs are more frequently observed with fs or ps pulses than with ns pulses.[1,65,90] Moreover, it was frequently observed that size distribution of NMs obtained with ns pulses is sharper than those obtained with ps and fs pulses.[1] This may be another effect of the improved homogeneity of plasma plume when it is temporally overlapped with the laser pulse.

With microsecond (μs) and millisecond (ms) pulses, thermal ablation mechanisms largely prevail, because material detachment takes place by vaporization and boiling, while the formation of a plasma plume is no longer required for LASiS.[46] A stream of melted nanodroplets and vaporized atoms is ejected from the target into the liquid solution, where three types of reactions may take place:[91,92] (i) vapour phase reactions between vapours of the target and of the solution, at temperature and pressure lower than in the plasma plume; (ii) liquid phase reactions between melted droplets from the target and the liquid solution; (iii) solid phase reactions between solidified drops from the target and the liquid solution. NMs

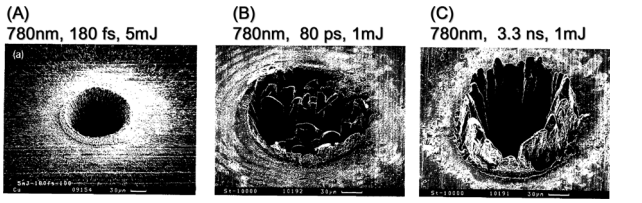

Fig. 9 Craters on metal targets after laser ablation in gas with fs (A), ps (B) and ns (C) pulses. Reprinted with permission from ref. 45.

Published on 01 November 2012. Downloaded by Universidade Federal do Parana on 22/05/2013 04:05:36.

obtained by ms pulses retain the typical signatures of vapour, liquid and solid phase reactions, like core–shell or hollow morphologies and heterostructures. For instance, the formation of hollow NPs by ms pulses is due to the Kirkendall effect, namely the outward motion of the boundary layer between the metal core and the oxide (or sulfide) shell, and it is compatible with reactions of type (ii) and (iii).[91,92] Interestingly, NMs obtained by ms laser ablation in liquids are polycrystalline like those obtained with shorter pulses.[91]

Spot area. When the spot area is increased by keeping the fluence unchanged, the NPs productivity also increases. In theory, one may expect that a larger spot area corresponds to a smoother gradient of temperature, pressure and concentration and, consequently, to a more homogeneous structure of the final products. However, the experimental results on LASiS of Au with ns laser pulses suggested that a larger spot area corresponds to a larger average size and size distribution of NPs, although these effects are not dramatic.[76,93] If more energy is delivered to the target by increasing the spot area, a larger amount of material is ablated and the concentration of target species in the plasma plume is higher, yielding larger nanoparticles. On the other hand, when more energy is delivered to the target, also the simultaneous occurrence of multiple ablation mechanisms is favoured, and it usually implies a broadening of the size distribution of NPs.[43,49] However, the effect of the spot area on the phase and structure of NPs has not been investigated systematically so far.

Repetition rate. The repetition rate defines the time interval (Δt_P) between consecutive laser pulses, with higher repetition rates corresponding to smaller Δt. The productivity of NPs for unit time increases with the repetition rate. However, linear increase is observed only for Δt_P longer than the lifetime of the cavitation bubble, which is of the order of 10^{-4}–10^{-3}s.[32] This corresponds to repetition rates lower than 10^3–10^4 Hz. The cavitation bubble is characterized by a discontinuity of refractive index at the liquid/gas interface, which causes scattering of laser light and reduces the laser energy reaching the target. Moreover, during the expansion of the cavitation bubble, laser ablation of the target takes place in a low density hot gaseous phase, similar to the case of laser ablation in gas. Therefore, confinement of plasma plume on the crater is less efficient and plasma etching of the target is diminished. These effects are limiting factors for high repetition rate laser ablation of the bulk target, which is the simplest strategy for improving LASiS productivity.[26,32] It is not clear what are the other possible modifications of the mechanism of NPs formation when the laser pulses overlap with the cavitation bubble.

Increasing the repetition rate also increases the local concentration of NPs in proximity of the crater, because the time for NPs diffusion away from the ablated region is reduced. This effect can favour the aggregation and the coalescence of NPs, but also the scattering of incoming laser pulses and the consequent decrease in the ablation yield.[87] On the other hand, for repetition rates of the order of kHz, the average temperature of the crater is sensibly higher than room temperature, therefore the fraction of matter that reaches the energy threshold for detachment during laser irradiation is larger and the ablation yield is improved compared to LASiS at room temperature.[26,32]

Number of laser pulses. The number of laser pulses is proportional to the ablation time, with proportionality constant given by the repetition rate. The amount of ablated material increases with the number of laser pulses, as reported systematically for the LASiS of AuNPs with ns laser pulses.[75] However, also the ablation product can change by increasing the number of laser pulses, especially if the bulk target undergoes modifications during laser ablation. Little experimental information is available on this point, which has been seldom considered in LASiS.[41] Target modification can be compositional, due to interaction with the molecules in solution, or morphological, due to the modification of the target surface by the detachment of material, and both these effects are favoured by the high temperature and pressure generated during laser ablation.[41] Compositional modification or simple contamination is possible also on relatively inert materials. For instance, the formation of defects by adsorption of organic byproducts can enhance the light absorption of the target and modify the ablation mechanism.[52] In the case of alloys, compositional modifications of the target may take place during LASiS, for instance because the crater becomes richer in the element with the highest heat of vaporization.[94] In such cases, the composition of NPs obtained by LASiS is continuously and dramatically affected by the number of laser pulses.

Morphological modifications influence the absorption properties of the target, with consequent change in the ablation yield and, eventually, of the ablation mechanism.[52] For instance, when the surface of a bulk target is polished, its reflectivity is increased and the absorbed energy is lower. Conversely, a rough surface absorbs more light, but not homogeneously in all its parts, with consequent inhomogeneities in the profile of the detached material.[52]

Unless the fresh liquid is continuously fluxed in the ablation cell, the concentration of NMs increases in solution for an increasing number of laser pulses. Since NPs scatter light, the net amount of energy delivered to the target decreases with the number of laser pulses. The special case of NPs that absorb laser light, for which further photoinduced modifications are possible, has been already mentioned in the "Pulse Wavelength" section.[1,86,87]

3.2 Material parameters

Solutes. Solutes can modify the physical–chemical properties of the liquid solution or can interact directly with the ablated material.

Solutes can modify the viscosity, the density and the surface tension of the solvent, which are relevant parameters for the dynamics of the cavitation bubble[58,73] and the confinement of the plasma plume on the crater.[64] In particular, the increase in solvent viscosity and density improves the confinement of the plasma plume on the ablated crater, which in turn enhances the ablation efficiency.[64] Bubbles may also template the aggregation of particles yielding hollow microspheres when NMs concentration is extremely high.[87] For instance, the addition of ethanol to water increased the viscosity of the liquid and improved the yield of hollow microspheres by prolongation of the bubbles' lifetime.[73] The literature does not provide any other insight into this topic, because solute-induced modification of solvent properties usually occurs as a side effect when solutes that interact directly with the NPs are added at high concentration to the solvent.[64,75,76] Therefore, the effect of the modification of physical–chemical properties of the liquid are veiled by the stronger effects due to the solute–NP interactions.

 This journal is © the Owner Societies 2013

Published on 01 November 2012. Downloaded by Universidade Federal do Parana on 22/05/2013 04:05:36.

The interaction between solutes and ablated material may have different degrees of intensity (Fig. 10a). At the smoothest level there are physical interactions, like sodium dodecyl sulfate (SDS) molecules with AuNPs obtained by LASiS in aqueous solution.[75,76,95] Dodecyl sulfate anions coordinate with the AuNPs surface by electrostatic interactions and form a molecular layer which limits both NPs coalescence and growth by adsorption of free atoms.[75,76] For instance, the size of AuNPs is reduced from 20 nm in pure water to *ca.* 10 nm in 10 mM SDS aqueous solution.[1,75] The size reduction is effective during NPs growth only if ligands concentration is large enough to compete with the diffusion of NPs embryos and of atomized target species. Also aggregation and precipitation of NPs is prevented by the use of SDS.[1] Similar effects are observed with cyclodextrins,[96] biopolymers,[88] polyvinylpyrrolidone[64] or cetyltrimethylammonium bromide.[93]

At a higher level of interaction there are ligands capable of chemical bonding with the surface of NPs, like thiolated molecules with AuNPs. When solutes establish chemical bonds with NPs, the capping action is irreversible and results in a very efficient limitation of NPs growth. For instance, AuNPs size can be reduced from 20 nm in pure water to 5–2 nm in millimolar thiol solutions.[1]

At the highest level of interaction between solutes and ablated material there are molecules that modify the composition of NPs (Fig. 10b). A simple case is LASiS of AuNPs in aqueous solution of NaCl.[1,65,97] Cl is present on the surface of such AuNPs due to the formation of Au–Cl chemical bonds. It has also been suggested that surface Cl atoms favour the dissociation of Au–O–Au bonds in $Au–O^-$ and Au–Cl groups, thus rising the NPs *Z*-potential and enhancing the stability of the colloidal system, especially at neutral and basic pH.[65] In general, NPs growth stops when the surface repulsion prevents the collision between particles or when, after the collision, the formation of interparticle chemical bonds is prevented.[76] In the case of NaCl, the high *Z*-potential enhances the surface repulsion among NPs and yields smaller particles compared to LASiS in pure water.[1] Similar results have been reported for LASiS of AgNPs with NIR pulses.[97] However, UV laser ablation of silver in aqueous solution of NaCl or KBr yields, respectively, AgCl cubic microstructures[28] or AgBr NPs.[98] In an aqueous solution of polysorbate, laser ablation of Ag yields Ag_2O microstructures with a mixture of shapes like cubes, pyramids, triangular plates, pentagonal rods, and bars.[99] The ablation conditions generated by UV pulses facilitate the reaction of Ag atoms with Cl, Br or O. Interestingly, when UV laser irradiation of Ag is performed in concentrated cetyltrimethylammonium bromide (CTAB) aqueous solution, layered AgBr–cetyltrimethylammonium compounds are obtained, due to the simultaneous effect of reaction between Ag and Br, promoted by UV pulses, and the assembly with surfactant molecules.[98]

Similar interactions between solutes and ablated materials are observed in other cases. For instance layered Zn hydroxide/dodecyl sulfate platelets are obtained by laser ablation of Zn in SDS aqueous solutions, while ZnO NPs are obtained if the same experiment is carried out in pure H_2O.[100] Interestingly, different doping of ZnO NPs was obtained by LASiS at different pH, with more surface defects produced at acidic pH and more lattice defects at basic pH.[101] This is the effect of the different concentration of H_3O^+ and OH^- ions in solution during formation of ZnO NPs.[101]

An open point about the role of solutes that chemically interact with the target material is that the reactions take place at the crater surface before, during and after the detachment of the ablated material. At the moment, the chemical evolution of the target composition during laser ablation is scarcely known, although its *ex situ* investigation by common surface characterization techniques is possible.

Finally, NPs can act as nucleation sites if solutes undergo spontaneous or temperature activated chemical reactions, because the temperature of the just formed NPs is higher than room temperature (Fig. 10c).[102] For instance, noble metal salts have been reduced on the surface of oxide or metal NPs *in situ* during LASiS, to yield core–shell, satellite or dimeric structures.[102]

Solvent. The solvent strongly influences the composition and the structure of NMs obtained by LASiS. This point is discussed first by considering the laser ablation of Au in different solvents, then moving gradually to more reactive materials like Ag and Fe. The comparison of Au, Ag and Fe is especially facilitated because we performed the laser ablation with 1064 nm (9 ns, 10 J cm^{-2}) pulses of such materials under the same experimental conditions, *i.e.* leaving all other parameters unchanged except for the solvent (Fig. 11).

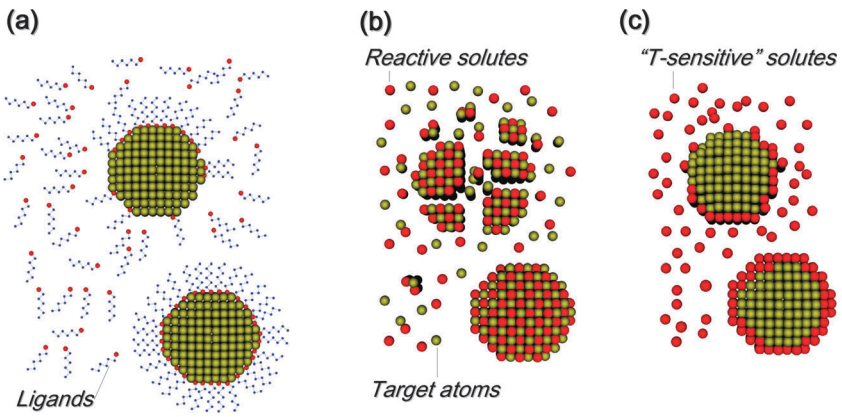

Fig. 10 Relevant examples of the solute effect on LASiS of NMs: (a) ligands absorb by physical or chemical interactions on the NPs surface by preventing their growth, coalescence, aggregation and, sometimes, precipitation; (b) solutes react with ablated material to yield a compound different from the bulk target; (c) solutes capable of temperature activated chemical reactions (''T-sensitive'' solutes) form new materials on the surface of the just formed NPs.

Published on 01 November 2012. Downloaded by Universidade Federal do Parana on 22/05/2013 04:05:36.

It is worth pointing out that the purity of a liquid is a relative concept and HPLC or spectroscopic grade solvents still contain atmospheric gases like N_2, O_2, H_2O and CO_2, and traces of other compounds. For instance, in water under atmospheric conditions there is about 9 mg dm^{-3} of O_2 and about 14 mg dm^{-3} of N_2.[103] The solubility of gases in other organic solvents is of the same order of magnitude.[104] In specific cases, the degradation over time of the solvent can yield byproducts (for instance peroxides in non-stabilized tetrahydrofuran). Therefore, in the following examples, one must take into account that impurities of various types are present during LASiS, even if spectroscopic or HPLC grade solvents were used.

Gold. The most well-known case of laser ablation in liquids is the LASiS of AuNPs in pure H_2O, which yields gold colloids stable for long time.[1] The surface of such AuNPs has been investigated by Meunier's[65] and Mafunè's[105] groups in order to understand the origin of the colloidal stability and both identified the presence of Au–O bonds as the possible reason. The presence of Au(I) atoms means that the synthesis conditions must be highly oxidising during LASiS. Oxygen is present both in H_2O, O_2 and CO_2 molecules, but increased colloidal stability has been reported for LASiS in water saturated with Ar or N_2, meaning that atmospheric O_2 or CO_2 may have detrimental effects on the surface oxidation process, probably by an electron scavenging effect.[106] This result highlights the importance of the proportion between ablated material and solution species and the great influence of chemical reactions between the ablated material and solvent impurities on the final product.

When laser ablation of the gold target is performed in organic solvents like ethanol (C_2H_6O), tetrahydrofuran (C_4H_8O), dimethylsulphoxide (C_2H_6OS), acetonitrile (C_2H_3N) and dimethylformamide (C_3H_7NO), crystalline metal AuNPs are obtained, as in the case of H_2O.[77,107] However, the average size of AuNPs is lower and the fraction of non-spherical and aggregated nanoparticles is larger than in H_2O.[77,107] In addition, coagulation and precipitation of AuNPs obtained in organic solvents is observed on the medium-long term.[77,107] The decrease in average NPs size can be due to a lower ablation efficiency, because the density of Au atoms detached from the target is lower, or to the capping effect originated by organic solvents, which hampers nuclei coalescence. Since the productivity of AuNPs in organic solvents is comparable or even higher than in H_2O, the first hypothesis should be excluded. Therefore, it is likely that solvent molecules (or byproducts of solvent molecules degraded in the ablation region) absorb on AuNPs and act as capping agents that prevents further NPs growth. Remarkably, Compagnini's group showed by Raman spectroscopy that laser ablation in organic solvents produces polyynes, which can absorb on the NPs surface.[108,109] In the case of LASiS of AuNPs in acetone (C_3H_6O), the formation of enolates and amorphous carbon was reported by Giorgetti and co-workers[110] and the formation of alcoholates was reported for the LASiS of Pd in ethanol by Cristoforetti and co-workers.[111] The authors suggested that the greater stability over time of NPs obtained in acetone and ethanol, compared to other organic solvents, may be explained by surface complexation with enolates and alcoholates, respectively, which are negatively charged molecules.[110,111] Hence, different solvents generate different byproducts with peculiar chemical and physical properties during laser ablation, and the determination of all these byproducts is not trivial.

In addition, the presence of non-spherical AuNPs is compatible with the incomplete coating of the particles surface with capping molecules, which allows the growth of nanocrystals only along the portion of the surface remaining uncovered. Since the AuNPs phase is crystalline, the capping species produced during LASiS in organic solvents cannot interfere with the formation of the fcc metal lattice, but can still adsorb on the nanocrystals surface in the later stage of their growth.

The lower stability of AuNPs obtained in organic solvents can be the combined effect of the lower dielectric constant, compared to H_2O, and of the lower Z-potential of NPs, due to absorption of solvent pyrolysis byproducts on their surface.[112] Also a lower surface oxidation of AuNPs could be expected in organic solvents compared to H_2O, although direct experimental evidence about this point is missing.

Laser ablation of Au in toluene (C_7H_8) is the most evident example of the capping action of byproducts generated by solvent degradation. The smallest AuNPs (average size of 1 nm) among all the solvents are obtained in toluene, and these NPs are embedded in a graphitic matrix.[113] All aromatic solvents undergo extended pyrolysis and yield graphitic materials when heated at *ca.* 10^3 K at low-oxygen concentration.[113] Therefore, the coalescence and growth of AuNPs is stopped in the early stage, when the average size is of a few nm, by the graphitic matrix due to toluene pyrolysis. Since Au has a rather null reactivity with C, crystalline metal AuNPs are formed anyway. Interestingly, several AuNPs are surrounded by a graphitic shell, probably because they acted as hot nucleation sites for the graphitization process. However, this is not the dominating mechanism of formation of the graphitic network, which is much more extended and completely embeds the small AuNPs. Thus, matrix formation initiates simultaneously and independently the formation of AuNPs nuclei. Otherwise, a denser matrix composed prevalently of larger AuNPs with a graphite shell nucleated on the hot surface of the particles would have been observed.[113]

When laser ablation of gold is performed in chloroform ($CHCl_3$), the reactivity of Au with Cl yields gold chloride ($AuCl_3$) NPs, while metal AuNPs are not obtained.[114] This suggests that nucleation and growth of NMs ablated from the target take place under conditions of high concentration of solvent molecules and the temperature and pressure above the threshold for chemical reaction between Au and $CHCl_3$. In principle, by considering the temperature threshold for the reaction between Au and $CHCl_3$, one may infer the lower temperature limit at which the extensive mixing of ablated material and solvent molecules occurs, although such a systematic study was not carried out.

When laser ablation of gold is performed in supercritical CO_2 or CHF_3, AuNPs are obtained as large aggregated fractal structures, with an average size of tens up to hundreds of nanometers.[115,116] Under supercritical conditions, enhanced confinement of the plasma plume is obtained by the high pressure and density of the liquid and physical–chemical properties of the liquid like thermal conductivity are modified, as discussed later in the section on "System Temperature and Pressure".

Laser ablation of gold in superfluid helium leads to the formation of nanowires composed of single AuNPs, arranged in

 This journal is © the Owner Societies 2013

Published on 01 November 2012. Downloaded by Universidade Federal do Parana on 22/05/2013 04:05:36.

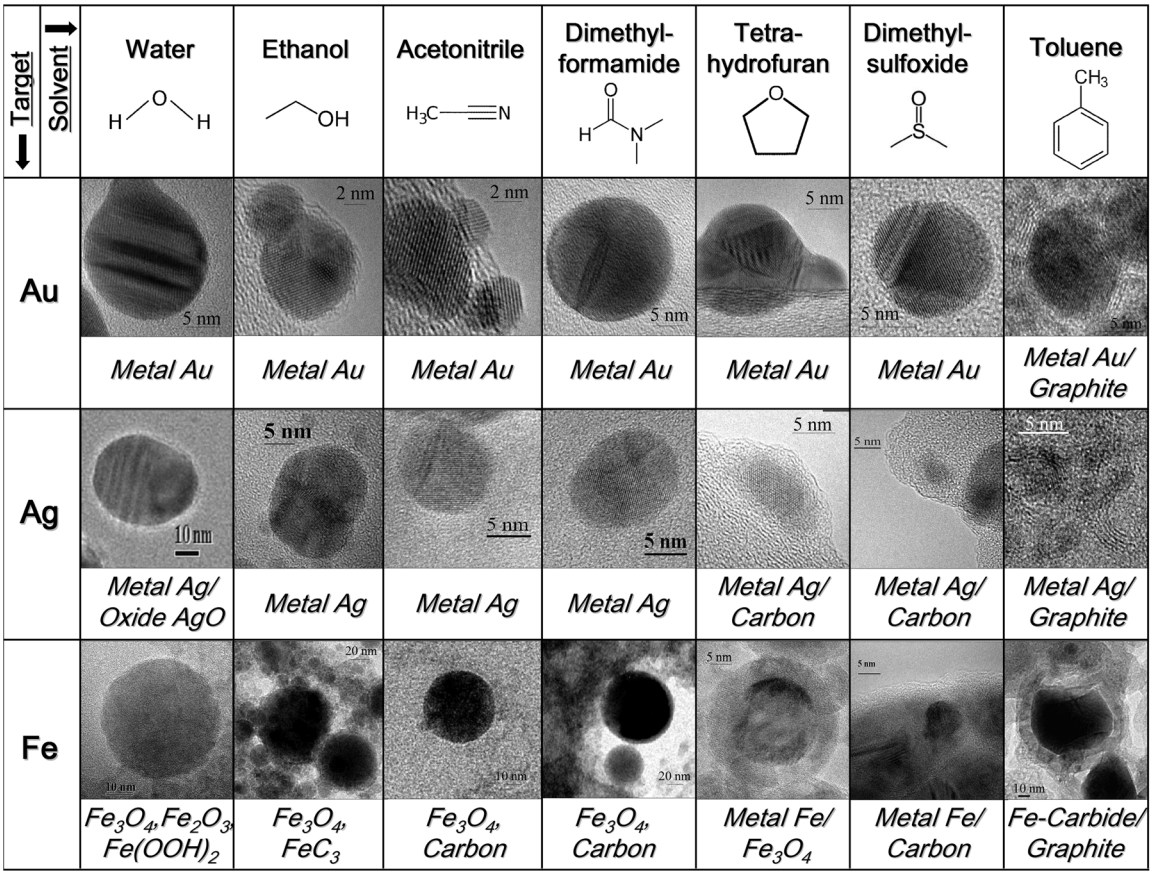

Fig. 11 Summary of the NMs obtained by laser ablation of Au, Ag and Fe bulk targets in different solvents with 9 ns pulses at 1064 nm and 10 J cm^{-2}. From ref. 16, 27, 30, 33, 34, 77, 113 and 118.

centimeter long networks.[117] The formation mechanism is likely due to the segregation of AuNPs in the quantized vortices of the superfluid liquid, which act as templates for the formation of macroscopic networks of nanowires.[117]

Silver. The parallel between laser ablation of gold and silver in different solvents is particularly informative. Silver is a noble metal with chemical and physical properties very similar to gold and both have scarce reactivity with carbon. However, the standard reduction potential of the Ag^+/Ag couple is 0.80 eV, while for the Au^+/Au couple is 1.69 eV. In fact, laser ablation of Ag in H_2O yields crystalline AgNPs with a thin passivating layer of Ag_2O, whose thickness increases with ageing of the colloidal solution.[1] Moreover, Ag_2O is partially soluble in water, and AgNPs undergo etching on a timescale of weeks.[1]

When laser ablation of Ag is performed in ethanol, acetonitrile and dimethylformamide, the results are similar to those of Au, namely crystalline AgNPs are obtained with smaller average size than in H_2O.[106,114,118] It suggests that the capping of degraded solvent molecules prevents NPs growth more effectively than surface oxidation, or that capping occurs simultaneously to nuclei coalescence while surface oxidation occurs on a longer timescale.

When laser ablation of Ag is performed in tetrahydrofuran, an amorphous shell around AgNPs is observed, likely due to solvent degradation, which causes the red shift of the surface plasmon resonance of silver nanoparticles.[118,119] The particles size is comparable to that of AgNPs obtained in the other organic solvents, thus the amorphous shell forms in the last stage of NPs formation, probably when particles are still hot enough to promote solvent pyrolysis but the growth process is already started.

In the case of dimethylsulphoxide, solvent degradation takes place simultaneously to AgNPs formation and on a large extent, with the formation of a thick amorphous matrix that completely embeds the metal particles.[118] Different results are obtained by laser ablation of Ag and Au targets in DMSO and THF, therefore the two metals must have a different chemistry under the experimental conditions of LASiS. Since Ag has a higher tendency to oxidation, it is possible that the concentration of oxidative species in the plasma plume is lower during ablation of silver than of gold, because part of Ag atoms react with O atoms. The lower concentration of oxygen may influence the reaction among solvent molecules under the high temperature and pressure conditions of laser ablation, for instance promoting the formation of networks of amorphous carbon instead of oxidised byproducts, which may have a lower tendency to networking. Importantly, some authors reported that ps laser irradiation of Ag with fluxed tetrahydrofuran produced AgNPs without the amorphous shell.[120] This information suggests that: (i) the formation of amorphous organic material may be related to the accumulation of ablation byproducts with time; (ii) the solvent byproducts do not accumulate on the target, but are prevalently produced in the solution, otherwise refreshing the liquid would not

Published on 01 November 2012. Downloaded by Universidade Federal do Parana on 22/05/2013 04:05:36.

provide any change (iii) solvent pyrolysis is reduced by using short (ps and fs) laser pulses, when thermal ablation mechanisms are less favoured and laser pulses do not overlap with plasma plume.

Laser ablation of Ag in toluene and in chloroform yields analogous results to what has been reported for Au.[33,114]

Iron. The case of iron provides further insight into the effect of solvents on LASiS, because it has the following features: (i) the reduction potentials are −0.41 V for the Fe^{2+}/Fe couple and 0.77 V for the Fe^{3+}/Fe^{2+} couple; (ii) Fe reacts with C giving carbides; (iii) Fe reacts with O giving various oxides like wustite (FeO), magnetite (Fe_3O_4), maghemite (γ-Fe_2O_3) and hematite (α-Fe_2O_3), while in the presence of H_2O it can give crystalline and amorphous hydroxides and mixed oxide–hydroxide phases.

The laser ablation of a Fe target in H_2O yields multiphase polycrystalline iron oxide NPs embedded in a amorphous hydroxide matrix.[16,27] The composition of the crystalline phases obtained under our experimental conditions was evaluated to be 75 wt% of Fe_3O_4, 22 wt% of α-Fe_2O_3, *ca.* 2 wt% of FeO and *ca.* 1 wt% of Fe.[16] In general, the composition of the final product depends on the local temperature and pressure as well as on the concentration of ablated material and solution molecules. Thanks to the peculiar chemistry of iron, a snapshot of these parameters is enclosed in the phase and structure of the obtained NPs. For instance, the presence of the amorphous iron hydroxide network is a clear indication that a fraction of ablated material is extracted as vapours/ions and reacts with an excess of water and oxygen to yield hydroxides at moderate temperature. It is known that heating Fe hydroxides yields Fe_3O_4 at 250–600 K and α-Fe_2O_3 at higher temperatures,[27,121,122] therefore the network is formed at lower temperatures than crystalline nanoparticles and, consequently, at higher H_2O concentration. Indeed, this is expected because the temperature gradient decreases on moving towards the solution, where the liquid molecules are present at higher concentration than the ablated material. A similar result, consisting of a gel of Pt hydroxides, is obtained by low fluence ns laser ablation of Pt in water.[41,43]

The prevalence of the Fe_3O_4 phase over the most oxidised α-Fe_2O_3 and the less oxidised FeO can be interpreted in two ways: (i) the concentration of Fe and O atoms is comparable when nucleation and growth of NPs take place, otherwise α-Fe_2O_3, FeO or Fe would have been obtained; (ii) the formation temperature of the 78 wt% of NPs (Fe_3O_4, FeO and Fe) is lower than that of the remaining 22 wt% (α-Fe_2O_3), since hematite is obtained only at high temperature in an oxidising environment.

Furthermore, the crystalline domains of 1 wt% of metal iron nanocrystals obtained by LASiS have a size of hundreds of nm, while the remaining 99 wt% of NPs is composed of iron oxide single domains of 3–10 nm.[16,27] This suggests that metal iron NPs result from the photomechanical detachment of large fragments or melted drops from the target, while oxide NPs prevalently derive from vaporization and ionization processes followed by nucleation and growth.

When the Fe target is ablated in ethanol, two types of NMs are observed: small (below 5 nm) Fe_3O_4 NPs and large (above 10 nm) FeC_3 NPs.[34] The occurrence of FeC_3 NPs is not surprising, since a similar result was obtained by electric plasma discharge of iron electrodes in ethanol.[34,123] However, the occurrence of two distinct populations of NMs (carbides and oxides) suggests that different formation conditions are required at different locations or at different times during LASiS. Iron oxide NPs are smaller than carbide NPs, suggesting that they are formed at longer times, when the temperature and the iron concentration are lower, and they can result from the reaction of iron with dissolved O_2 or O atoms from the ethanol molecules. Conversely, iron carbide NPs form only at low oxygen concentration and in the presence of pyrolysed ethanol molecules, which requires high temperature.[123] In the plasma plume, high T is associated with high C_M, hence the formation of large carbide NPs is possible, instead of oxide NPs. An alternative explanation is that the target itself modifies the composition from metal iron into iron carbide during the ablation process, hence the direct ablation of carbide nanoparticles occurs, giving as a side product the iron oxide NPs.

Laser ablation of the Fe target in organic solvents like acetonitrile and dimethylformamide prevalently yields magnetite NPs, similar to what is observed in water, but iron hydroxides are not obtained because water may be present only as an impurity.[34] Amorphous carbon is observed as a side product of LASiS, especially in dimethylformamide, although NPs are not embedded in it. Iron carbides have not been observed, and one can speculate that acetonitrile and dimethylformamide molecules are more prone to react with oxygen dissolved in solution than with Fe atoms.

Laser ablation of Fe in tetrahydrofuran yields *ca.* 20% of magnetite NPs, as in acetonitrile and dimethylformamide, and 80% of NPs with core–shell α-Fe–Fe_3O_4 structure.[34] The size of these NPs is comparable to that of larger oxide particles obtained in the other solvents and both cores and shells are polycrystalline. Since NP cores are composed of metal iron instead of iron oxide or carbide, the concentration of oxygen and carbon must be very low compared to that of iron when the nucleation and growth occur. It is possible that the C and O concentration is maintained low by the prompt reaction of solvent molecules with dissolved oxygen during the formation of FeNPs. Alternatively, metal cores can form by the direct ejection of melted drops from the target, similar to LASiS with ms pulses.[91] If the ablation mechanism is dominated by the ejection of melted droplets, contrariwise to the other solvents, then it must be due to different physical–chemical properties of THF, like thermal conductivity, viscosity, concentration of dissolved oxygen and refractive index. However, physical–chemical properties of tetrahydrofuran are average of those of the other organic solvents, hence the hypothesis about the ejection of melted drops cannot be explained easily.

In dimethylsulphoxide, laser ablation of iron gives an amorphous thick matrix embedding metal iron NPs.[34] Since iron oxide NPs are not observed, the organic matrix forms very early, just after nucleation of FeNPs. This finding is similar to what was observed for silver and suggests that laser ablation of metals with low reduction potential is a requisite for the formation of the amorphous carbon matrix in dimethylsulfoxide.

In toluene, the graphitic matrix due to solvent pyrolysis is observed, as already reported for Ag and Au.[34] However, 100% of amorphous iron carbide NPs are obtained, meaning that byproducts of toluene pyrolysis are more reactive with iron than

 This journal is © the Owner Societies 2013

Published on 01 November 2012. Downloaded by Universidade Federal do Parana on 22/05/2013 04:05:36.

dimethylsulfoxide byproducts. As discussed about laser ablation of Au and Ag, pyrolysis of organic solvents generates different byproducts with different chemical and physical properties like, for instance, alcoholates from ethanol and graphite from toluene. Hence, the presence of C or O in the molecular structure of the solvent is not enough to rationalize the variety of phases and structures obtained by laser ablation of Fe in different environments (Fig. 11). In particular, experimental results indicate that one must consider the reactivity of solvent molecules (and their pyrolysis byproducts) with the ablated material, with the oxygen dissolved in solution and with the other molecules of solvent, all together. The influence of the solvent on the physical state of detached material also deserves further clarification.

3.3 Bulk target

The comparison of literature results for different target materials is not straightforward, because physical and chemical effects are mixed and experimental parameters (for instance the use of water or of organic solvents) are not homogeneous. However in most cases, it is possible to find analogies, especially when target materials with similar chemical–physical properties are ablated. Hence, in this paragraph we grouped the results according to the material composing the bulk target.

Metals. Many similarities between laser ablation of Fe and of other transition metals are found in the literature, although direct comparison may be complicated due to the different experimental parameters.

Laser ablation of Co in water yields cobalt oxides, while in hexane metal CoNPs are obtained.[124] In toluene, amorphous cobalt carbide NPs embedded in the graphitic matrix are found,[125] with the same morphology as that observed for Fe. Metal Co and Ni NPs are obtained by laser ablation of the bulk metal targets in deaerated ethylene glycol solution of polyvinylpyrrolidone.[126]

Laser ablation of Cr in water yields dodecahedral and tetragonal Cr_3O_4 and corundum-type Cr_2O_3. The Cr_3O_4 phases are affected by internal compressive stress due to doping with Cr^{2+}, Cr^{3+}, and H^+, which modify their optoelectronic properties.[127]

Metal CuNPs can be obtained by LASiS in acetone,[128] while laser ablation of Cu in water yields copper oxide NPs.[128,129] Large (*ca.* 100 nm) CuO NPs are prevalently obtained at high fluence, while small (*ca.* 10 nm) Cu_2O NPs are the dominant product at lower fluence.[129] The application of a DC electric field during LASiS templates the formation of CuO NPs into polycrystalline nanometric spindle shapes (Fig. 12a).[130]

Laser ablation of Mn in H_2O yields Mn_3O_4 nanostructured agglomerates by reaction of Mn atoms with the oxidising solution environment.[131] Targets of Sn and Ti under the same conditions yield oxide NPs with various stoichiometries, similar to the case of Fe.[132–134] Laser ablation of Ti in 2-propanol and hexane produces titanium carbide NPs, while in ethanol a mixture of oxides and carbides was obtained,[132] in analogy to the case of iron.

As discussed above, laser ablation of Zn in water and in several organic solvents like tetrahydrofuran yields zinc oxides.[101,135] Interestingly, the formation of zinc oxide NPs by LASiS in tetrahydrofuran solution of ε-caprolactone promotes the oligomerization of the monomer, simultaneously to solvent pyrolysis.[135] Olefinic byproducts were prevalently found by LASiS with ps and fs pulses, while carbonylic byproducts were prevalently found with ns pulses.[135]

Laser ablation of Ta in ethanol yields tantalum oxide NPs coated with a passivating amorphous shell identified as Ta_2O_5.[136]

The laser ablation of W in water is peculiar because the ablated material strongly reacts with H_2O molecules yielding isopolyanions of tungsten oxide, which aggregate and further polymerize at longer times after the LASiS.[137] Such a phenomenon recalls the case of laser ablation of Pt at low fluence, where Pt hydroxides are prevalently obtained,[41] and is especially favoured when the concentration of target species is low compared to solvent molecules, which may occur especially with a refractory material like W.

Laser ablation of Zr in water yields monoclinic zirconia NPs, while cubic zirconia NPs are obtained in ammonia.[138]

Laser ablation of Mg in water yields brucite $Mg(OH)_2$ NPs, while in 2-propanol and acetone a mixture of MgO and metal Mg NPs is obtained.[139]

Laser ablation of Al in ethanol yields polycrystalline Al NPs embedded in an oxide matrix.[140] Interestingly, the thickness of the oxide matrix is reduced when ultrashort laser pulses (fs) are used.[140] When laser ablation is performed in ethanol saturated by gaseous hydrogen, core–shell Al–Al_2O_3 NPs are obtained and the two layers are separated by an intermediate amorphous shell (Fig. 12b).[36]

Laser ablation of Ga in H_2O solution of CTAB yields GaOOH NPs which grow with a spindle-like shape upon ageing, while amorphous gallium hydroxides are obtained in pure water or in SDS solution.[141]

Laser ablation of In in water yields In_2O_3 crystalline NPs and amorphous byproducts,[142] while laser ablation of Pb in liquid mercaptans yields hollow PbS NPs by a nanoscale Kirkendall process (Fig. 12c).[91]

Carbon. Laser ablation of C-graphite in water yields a mixture of graphite particulates, amorphous carbon, polyynes and, at very high fluence, also nanodiamond materials.[37,71,108,109] The formation mechanism of nanodiamonds is correlated with the high pressure generated during laser ablation,[37] which affects the plasma plume but also the surface of the target. Actually, nanodiamonds are nucleated in the crater of amorphous carbon targets, because of the effect of the high pressure generated during 532 nm ns laser ablation in H_2O at high fluence.[143] This finding supports the hypothesis that, in LASiS, nuclei of NMs can be extracted from the target instead of being formed by a nucleation process during the expansion and cooling of the atomized species in the plasma plume.

Semiconductors. The laser ablation of silicon in chloroform yields polycrystalline NPs with an average size of about 50 nm, composed of small crystalline domains with a size of 3–5 nm,[144] which is a structure similar to iron oxide NPs obtained by LASiS in H_2O.[16,27] The small domains are embedded in an amorphous silicon oxide matrix produced by reaction of Si atoms with oxygen dissolved in the liquid solution.[144] Laser ablation in ethanol yields a mixture of polycrystalline Si NPs embedded in a SiO_2 matrix and a minority of SiC NPs,[145] while Si cores passivated by an oxide shell are obtained in water.[146] Interestingly, when laser ablation of silicon is performed in deaerated 1-octene, a monolayer of solvent molecules coats the SiNPs by forming covalent bonds between octene C

Published on 01 November 2012. Downloaded by Universidade Federal do Parana on 22/05/2013 04:05:36.

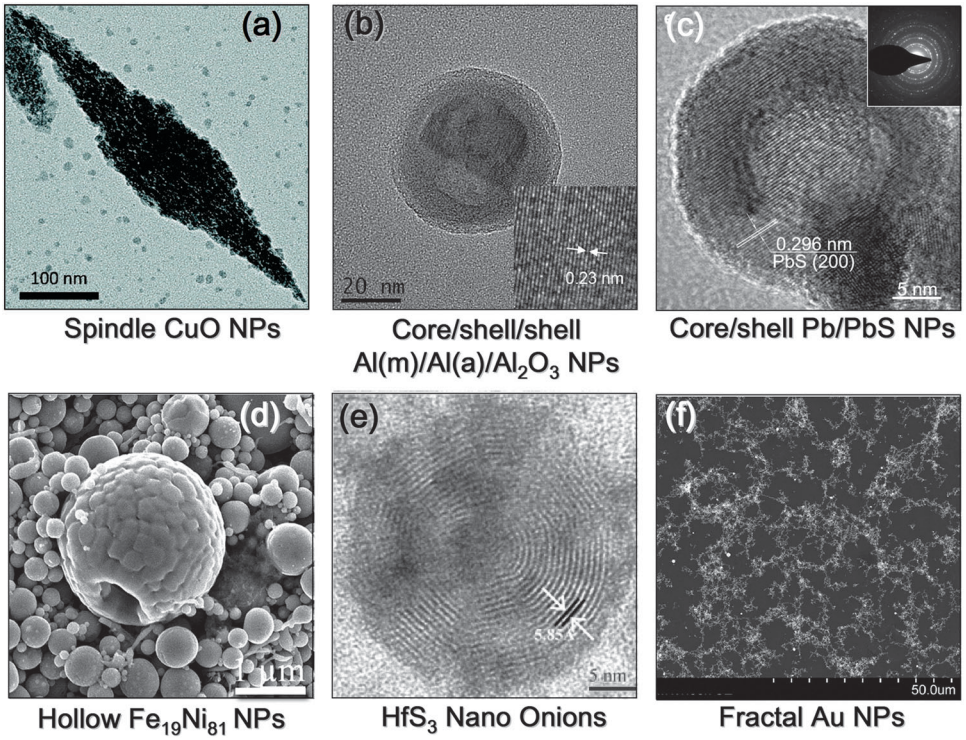

Fig. 12 Interesting examples of NMs obtained by LASiS: (a) CuO nanospindle obtained by ns pulses at 532 nm in water in a DC electric field (ref. 130); (b) core–shell–shell metal Al–amorphous Al–Al_2O_3 (Al(m)–Al(a)–Al_2O_3) obtained by ps laser ablation at 1064 nm in ethanol (ref. 36); (c) core–shell Pb–PbS NPs obtained by 1064 nm ms pulses in mercaptan solutions (ref. 91); (d) hollow permalloy spheres obtained by 248 nm ns pulses in SDS aqueous solution (ref. 87); (e) Hf_2S nano onions obtained by 532 nm ns pulses in *tert*-butyl disulfide (ref. 161); (f) fractal AuNPs obtained by 532 nm ns pulses in supercritical CO_2 (ref. 116). All figures (a), (b), (c), (d), (e) and (f) are reprinted with permission from ref. 36, 91, 87, 116, 130, and 161 respectively.

atoms and surface Si atoms.[35] The formation of Si radicals on the surface of Si NPs is crucial for the reaction with octene molecules.[35]

Laser ablation of a single crystalline Ge target in H_2O under the application of a DC electric field yields GeO_2 micro and nano particles with various shapes (spheres, cubes, spindles).[147] By performing the same synthesis in toluene, tetragonal Ge compounds are produced, which is a metastable phase obtainable only at high pressure.[148]

Laser ablation of Cd in water yields cadmium hydroxide NPs, which assemble on a longer timescale into nanorods, nanotetrapods and nanoflowers when SDS is present in solution.[38]

Laser ablation of Si-doped GaAs in water and ethanol yields zinc blend GaAs NPs passivated by an oxide layer embedded in mixed amorphous oxides.[149] Similarly, the products of the laser ablation of bulk CdS and ZnSe in organic solvents contain also CdS and ZnSe nanostructures,[150] and partially oxidised CdTe, CdSe and ZnTe NPs are obtained by laser ablation of the corresponding bulk targets in methanol.[151]

Metal alloys. A limited set of experiments concerns laser ablation of metal alloys in liquids, although they provide information on the correlation between the stoichiometry of the bulk target and of the final alloy NPs. Laser ablation of noble metal alloys like PtAu in H_2O and PtIr in acetone gives NPs with stoichiometry very similar to that of the target.[13,152] In the case of transition metals like NiFe and, particularly, SmCo, the stoichiometry of NPs differs from that of the target and varies with the solvent used.[94] It may be interpreted either as the difference between the latent evaporation heats (Δ_H) of 56% for Sm–Co and of 10% for Ni–Fe, or as the different reactivity with solvent and oxygen molecules of the elements composing the alloy.[94] Since also noble metal alloys like Pt–Au or Pt–Ir have different evaporation heats (Δ_H = −31% and +20% respectively), the hypothesis concerning the different reactivity of the elements with solution molecules seems to be more probable. The LASiS of FePt alloy NPs in hexane and water further confirms this hypothesis, since Δ_H = 27% but the stoichiometry is not retained.[153]

Laser ablation of a permalloy ($Fe_{19}Ni_{81}$) target in SDS aqueous solution can yield hollow permalloy NPs with a size of *ca.* 500 nm (Fig. 12d) because, simultaneously to LASiS, already formed NPs are photofragmented and gas bubbles produced during the process act as templates for their reassembly.[87]

Oxides. Laser ablation of doped oxides (Y_2O_3:Eu^{3+}, Gd_2O_3:Eu^{3+} and $Y_3Al_5O_{12}$:Ce^{3+}) in aqueous solution of polyethers yields "cubic disordered" phases (for Y_2O_3:Eu^{3+}, Gd_2O_3:Eu^{3+}) or a mixture of α-Al_2O_3, $Y_3Al_5O_{12}$ and a minority of $YAlO_3$ NPs (for $Y_3Al_5O_{12}$:Ce^{3+}), respectively, by maintaining the initial doping.[154] Interestingly, the polyether stabilizes the NMs by surface coordination of metal ions with bidentate carboxylate ($-COO^-$) groups.[154] Similarly, NPs of Lu_2O_2S:Eu^{3+}, Gd_2SiO_5:Ce^{3+}, Lu_3TaO_7:Gd^{3+}, Lu_3TaO_7:Tb^{3+} [155] and $Tb_3Al_5O_{12}$:Ce^{3+} [156] can be synthesized by laser ablation in aqueous solutions of the bulk target with the same composition.

 This journal is © the Owner Societies 2013

Published on 01 November 2012. Downloaded by Universidade Federal do Parana on 22/05/2013 04:05:36.

Laser ablation of the phosphor $Sr_2MgSi_2O_7$:Eu,Dy in ethanol successfully yields 83% of NMs with composition of the target and 17% of $Sr(HCOO)_2$ as a by-product.[157]

Laser ablation of vanadate ($M_xV_yO_n$ where M is a transition metal) can be exploited for the preparation of various copper vanadate nanostructures,[158] and laser ablation of the bismuth oxide target in ethanol yields monoclinic Bi_2O_3 NPs.[159]

Laser ablation of $Ca_{10}(PO_4)_6(OH)_2$ (hydroxyapatite) in water yields defective hydroxyapatite NPs with an excess of surface Ca atoms but, interestingly, LASiS yields a more stoichiometric product than laser ablation in gas phase.[160]

Other compounds. Laser ablation of MoS_2 in water yields MoS_2 onion-like nanospheres with an amorphous core composed of amorphous molybdenum oxide, which act as nucleation sites for the layered shell.[6,39] If laser ablation of MoS_2 is performed in an oxygen-free liquid like *n*-decane, it does not yield the layered onion-like structure, because the amorphous Mo oxide nucleation sites do not form.[39] A similar formation mechanism is observed for onion-like Hf_2S NPs obtained by laser ablation of HfS_3 in *tert*-butyl disulfide (Fig. 12e).[161]

Laser ablation of hexagonal boron nitride (h-BN) targets yields products with different morphology like nanospheres, nanoflakes and nanoscrolls of the hexagonal phase, as well as NPs of cubic or orthorhombic BN, depending on the laser fluence adopted for the LASiS.[162,163] The formation mechanism is similar to that observed in laser ablation of graphite targets.[162,163]

3.4 System temperature and pressure

The range of temperatures and pressures allowed for the experimental set up of LASiS is limited compared to the values reached in the ablation region, therefore minor effects on NMs formation are expected by variation of such parameters.

Temperature affects several physical properties of liquids like viscosity, density, refractive index, surface tension and compressibility, which in turn alter the efficiency of laser irradiation, plasma plume confinement and the cavitation bubble dynamics.[72–74,164] In particular, the hydrodynamic size of AuNPs aggregates obtained by LASiS in H_2O was correlated with liquid temperature as the effect of the variation of liquid compressibility.[164]

The effect of external pressure on LASiS can be investigated only by using a specific experimental set up, which is usually applied to laser ablation in supercritical fluids. Au and Si targets have been ablated in common supercritical fluids like CO_2 and CHF_3 (Fig. 12f).[115,116,165] In such cases, no dramatic differences have been reported by changing the liquid pressure, except that larger particles are obtained at larger pressure, probably because the ablation efficiency is improved by the more effective plasma confinement on the crater.[115,116,165] Upon increasing the pressure, the cooling rate of ablated material increases,[165] while the lifetime of the cavitation bubble and its maximum size decrease.[166] How these effects influence the structure of NMs obtained by LASiS is not well understood at the moment, although it has been reported that Si NPs have more defects when obtained at high pressure, *i.e.* when the cooling rate is higher.[165] More results are expected in the future by the use of dedicated cells for the real time investigation of the ablation process at different pressures.[82]

4. Conclusions

A library of nanomaterials with interesting structure and peculiar properties is disclosed by LASiS. Currently, this technique is evolving from the initial stage, in which research efforts were focused on the characterization of products, towards an advanced stage aimed at obtaining a full quantitative picture of the whole synthetic process. Such advancement is necessary to govern the variety of products that can be obtained by LASiS and requires a thorough understanding of the physical and chemical processes involved in the synthesis. However, several pieces of this puzzle are still missing, and they can be found only by multidisciplinary investigation skills.

In this perspective, we summarized the main physical–chemical stages of laser ablation in liquids, organized according to their temporal sequence, and we provided a list of examples, derived from the rich library accessible by this technique, about the correlation between experimental parameters of LASiS and the formation of NMs. The discussion can guide the LASiS of NMs with the desired phase, composition and structure and highlights several issues requiring further clarification. In particular, the molecular species and the chemical reactions which participate in LASiS are largely unknown. The accurate quantitative determination of the space–time profiles of temperature, pressure, concentration of the ablated material and concentration of the species in solution is crucial to understand what really happens during LASiS and to control the phase and structure of its products.

Acknowledgements

Financial support from the University of Padova is acknowledged (PRAT no. CPDA114097/11).

References

1 V. Amendola and M. Meneghetti, *Phys. Chem. Chem. Phys.*, 2009, **11**, 3805–3821.
2 V. Amendola, M. Meneghetti, S. Fiameni, S. Polizzi, G. Fracasso, A. Boscaini and M. Colombatti, *Anal. Methods*, 2011, **3**, 849–856.
3 V. Amendola and M. Meneghetti, *Adv. Funct. Mater.*, 2012, **22**, 353–360.
4 V. Amendola, G. Mattei, C. Cusan, M. Prato and M. Meneghetti, *Synth. Met.*, 2005, **155**, 283–286.
5 V. Amendola, D. Dini, S. Polizzi, J. Shen, K. M. Kadish, M. J. F. Calvete, M. Hanack and M. Meneghetti, *J. Phys. Chem. C*, 2009, **113**, 8688–8695.
6 H. Wu, R. Yang, B. Song, Q. Han, J. Li, Y. Zhang, Y. Fang, R. Tenne and C. Wang, *ACS Nano*, 2011, **5**, 1276–1281.
7 A. Pasquazi, S. Stivala, G. Assanto, V. Amendola, M. Meneghetti, M. Cucini and D. Comoretto, *Appl. Phys. Lett.*, 2008, **93**, 091111.
8 E. Messina, E. Cavallaro, A. Cacciola, R. Saija, F. Borghese, P. Denti, B. Fazio, C. D'Andrea, P. G. Gucciardi, M. A. Iati, M. Meneghetti, G. Compagnini, V. Amendola and O. M. Marago, *J. Phys. Chem. C*, 2011, **115**, 5115–5122.

Published on 01 November 2012. Downloaded by Universidade Federal do Parana on 22/05/2013 04:05:36.

9 E. Messina, E. Cavallaro, A. Cacciola, M. A. Iati, P. G. Gucciardi, F. Borghese, P. Denti, R. Saija, G. Compagnini, M. Meneghetti, V. Amendola and O. M. Marago, *ACS Nano*, 2011, **5**, 905–913.
10 V. Morandi, F. Marabelli, V. Amendola, M. Meneghetti and D. Comoretto, *J. Phys. Chem. C*, 2008, **112**, 6293–6298.
11 V. Morandi, F. Marabelli, V. Amendola, M. Meneghetti and D. Comoretto, *Adv. Funct. Mater.*, 2007, **17**, 2779–2786.
12 A. Hahn, S. Gunther, P. Wagener and S. Barcikowski, *J. Mater. Chem.*, 2011, **21**, 10287–10289.
13 J. Jakobi, A. Menéndez-Manjón, V. S. K. Chakravadhanula, L. Kienle, P. Wagener and S. Barcikowski, *Nanotechnology*, 2011, **22**, 145601.
14 J. Liu, C. Liang, H. Zhang, Z. Tian and S. Zhang, *J. Phys. Chem. C*, 2012, **116**, 4986–4992.
15 P. Liu, Y. Liang, X. Lin, C. X. Wang and G. Yang, *ACS Nano*, 2011, **5**, 4748–4755.
16 V. Amendola, M. Meneghetti, G. Granozzi, S. Agnoli, S. Polizzi, P. Riello, A. Boscaini, C. Anselmi, G. Fracasso and M. Colombatti, *J. Mater. Chem.*, 2011, **21**, 3803–3813.
17 M. Meneghetti, A. Scarsi, L. Litti, G. Marcolongo, V. Amendola, M. Gobbo, M. Di Chio, A. Boscaini, G. Fracasso and M. Colombatti, *Small*, 2012, DOI: 10.1002/smll.201200614, in press.
18 T. E. Itina, *J. Phys. Chem. C*, 2011, **115**, 5044–5048.
19 H. Wang, A. Pyatenko, K. Kawaguchi, X. Li, Z. Swiatkowska-Warkocka and N. Koshizaki, *Angew. Chem.*, 2010, **122**, 6505–6508.
20 T. Asahi, T. Sugiyama and H. Masuhara, *Acc. Chem. Res.*, 2008, **41**, 1790–1798.
21 D. Werner, T. Ueki and S. Hashimoto, *J. Phys. Chem. C*, 2012, **116**, 5482–5491.
22 V. Amendola and M. Meneghetti, *J. Mater. Chem.*, 2007, **17**, 4705–4710.
23 L. V. Zhigilei, Z. Lin and D. S. Ivanov, *J. Phys. Chem. C*, 2009, **113**, 11892–11906.
24 H. Ushida, N. Takada and K. Sasaki, *Diagnostics of liquid-phase laser ablation plasmas by spectroscopic methods*, IOP Publishing, 2007.
25 C. J. Murphy, *J. Mater. Chem.*, 2008, **18**, 2173–2176.
26 C. L. Sajti, R. Sattari, B. N. Chichkov and S. Barcikowski, *J. Phys. Chem. C*, 2010, **114**, 2421–2427.
27 V. Amendola, P. Riello, S. Polizzi, S. Fiameni, C. Innocenti, C. Sangregorio and M. Meneghetti, *J. Mater. Chem.*, 2011, **21**, 18665–18673.
28 Z. Yan, G. Compagnini and D. B. Chrisey, *J. Phys. Chem. C*, 2011, **115**, 5058–5062.
29 F. Mastrotto, P. Caliceti, V. Amendola, S. Bersani, J. P. Magnusson, M. Meneghetti, G. Mantovani, C. Alexander and S. Salmaso, *Chem. Commun.*, 2011, **47**, 9846–9848.
30 V. Amendola and M. Meneghetti, *J. Phys. Chem. C*, 2009, **113**, 4277–4285.
31 S. Salmaso, P. Caliceti, V. Amendola, M. Meneghetti, J. P. Magnusson, G. Pasparakis and C. Alexander, *J. Mater. Chem.*, 2009, **19**, 1608–1615.
32 P. Wagener, A. Schwenke, B. N. Chichkov and S. Barcikowski, *J. Phys. Chem. C*, 2010, **114**, 7618–7625.
33 V. Amendola, S. Polizzi and M. Meneghetti, *Sci. Adv. Mater.*, 2012, **3**, 497–500.
34 V. Amendola, P. Riello and M. Meneghetti, *J. Phys. Chem. C*, 2011, **115**, 5140–5146.
35 N. Shirahata, M. R. Linford, S. Furumi, L. Pei, Y. Sakka, R. J. Gates and M. C. Asplund, *Chem. Commun.*, 2009, 4684–4686.
36 G. Viau, V. Collire, L. Lacroix and G. A. Shafeev, *Chem. Phys. Lett.*, 2011, **501**, 419–422.
37 C. X. Wang, P. Liu, H. Cui and G. W. Yang, *Appl. Phys. Lett.*, 2005, **87**, 201913.
38 S. C. Singh and R. Gopal, *J. Phys. Chem. C*, 2010, **114**, 9277–9289.
39 G. Compagnini, M. G. Sinatra, G. C. Messina, G. Patanè, S. Scalese and O. Puglisi, *Appl. Surf. Sci.*, 2012, **258**, 5672–5676.
40 L. Berthe, R. Fabbro, P. Peyre and E. Bartnicki, *J. Appl. Phys.*, 1999, **85**, 7552–7555.
41 W. T. Nichols, T. Sasaki and N. Koshizaki, *J. Appl. Phys.*, 2006, **100**, 114913.
42 A. V. Kabashin and M. Meunier, *J. Appl. Phys.*, 2003, **94**, 7941–7943.
43 W. T. Nichols, T. Sasaki and N. Koshizaki, *J. Appl. Phys.*, 2006, **100**, 114912.
44 R. Fabbro, J. Fournier, P. Ballard, D. Devaux and J. Virmont, *J. Appl. Phys.*, 1990, **68**, 775–784.
45 C. Momma, B. N. Chichkov, S. Nolte, F. von Alvensleben, A. Tünnermann, H. Welling and B. Wellegehausen, *Opt. Commun.*, 1996, **129**, 134–142.
46 A. Miotello and R. Kelly, *Appl. Phys. A: Mater. Sci. Process.*, 1999, **69**, 67–73.
47 M. Hashida, H. Mishima, S. Tokita and S. Sakabe, *Opt. Express*, 2009, **17**, 13116–13121.
48 D. Perez and L. J. Lewis, *Phys. Rev. B: Condens. Matter Mater. Phys.*, 2003, **67**, 184102.
49 D. Perez, L. K. Béland, D. Deryng, L. J. Lewis and M. Meunier, *Phys. Rev. B: Condens. Matter Mater. Phys.*, 2008, **77**, 014108.
50 L. V. Zhigilei, P. B. S. Kodali and B. J. Garrison, *J. Phys. Chem. B*, 1998, **102**, 2845–2853.
51 L. V. Zhigilei, E. Leveugle, B. J. Garrison, Y. G. Yingling and M. I. Zeifman, *Chem. Rev.*, 2003, **103**, 321–348.
52 W. T. Nichols, T. Sasaki and N. Koshizaki, *J. Appl. Phys.*, 2006, **100**, 114911.
53 P. Lorazo, L. J. Lewis and M. Meunier, *Phys. Rev. Lett.*, 2003, **91**, 225502.
54 P. Lorazo, L. J. Lewis and M. Meunier, *Phys. Rev. B: Condens. Matter Mater. Phys.*, 2006, **73**, 134108.
55 F. Giammanco, E. Giorgetti, P. Marsili and A. Giusti, *J. Phys. Chem. C*, 2010, **114**, 3354–3363.
56 Y. Sano, N. Mukai, K. Okazaki and M. Obata, *Nucl. Instrum. Methods Phys. Res., Sect. B*, 1997, **121**, 432–436.
57 A. Vogel, N. Linz, S. Freidank and G. Paltauf, *Phys. Rev. Lett.*, 2008, **100**, 38102.
58 Y. Tomita, M. Tsubota and N. An-naka, *J. Appl. Phys.*, 2003, **93**, 3039–3048.
59 T. Tsuji, Y. Tsuboi, N. Kitamura and M. Tsuji, *Appl. Surf. Sci.*, 2004, **229**, 365–371.

 This journal is © the Owner Societies 2013

Published on 01 November 2012. Downloaded by Universidade Federal do Parana on 22/05/2013 04:05:36.

60 T. Sakka, S. Iwanaga, Y. H. Ogata, A. Matsunawa and T. Takemoto, *J. Chem. Phys.*, 2000, **112**, 8645–8653.
61 T. Sakka, K. Takatani, Y. H. Ogata and M. Mabuchi, *J. Phys. D*, 2002, **35**, 65.
62 L. V. Zhigilei, *Appl. Phys. A: Mater. Sci. Process.*, 2003, **76**, 339–350.
63 J. H. Yoo, S. H. Jeong, X. L. Mao, R. Greif and R. E. Russo, *Appl. Phys. Lett.*, 2000, **76**, 783–785.
64 T. Tsuji, D.-. Thang, Y. Okazaki, M. Nakanishi, Y. Tsuboi and M. Tsuji, *Appl. Surf. Sci.*, 2008, **254**, 5224.
65 J. P. Sylvestre, S. Poulin, A. V. Kabashin, E. Sacher, M. Meunier and J. H. T. Luong, *J. Phys. Chem. B*, 2004, **108**, 16864–16869.
66 N. Haustrup, X. Sedao, A. J. Conneely and G. M. O'Connor, *J. Phys. Chem. C*, 2011, **115**, 5028–5037.
67 G. A. Ozin, A. C. Arsenault and L. Cademartiri, *Nanochemistry: a chemical approach to nanomaterials*, Royal Society of Chemistry, 2008.
68 L. Kiss, J. Söderlund, G. Niklasson and C. Granqvist, *Nanotechnology*, 1999, **10**, 25.
69 J. Söderlund, L. Kiss, G. Niklasson and C. Granqvist, *Phys. Rev. Lett.*, 1998, **80**, 2386.
70 A. De Giacomo, M. Dell'Aglio, O. De Pascale and M. Capitelli, *Spectrochim. Acta, Part B*, 2007, **62**, 721–738.
71 A. De Giacomo, A. De Bonis, M. Dell'Aglio, O. De Pascale, R. Gaudiuso, S. Orlando, A. Santagata, G. Senesi, F. Taccogna and R. Teghil, *J. Phys. Chem. C*, 2011, **115**, 5123–5130.
72 D. G. Shchukin and H. Mohwald, *Phys. Chem. Chem. Phys.*, 2006, **8**, 3496–3506.
73 Z. Yan, R. Bao, Y. Huang and D. B. Chrisey, *J. Phys. Chem. C*, 2010, **114**, 11370–11374.
74 R. Zhao, R. Xu, Z. Shen, J. Lu and X. Ni, *Opt. Laser Technol.*, 2007, **39**, 968–972.
75 Mafunè Fumitaka, J. Kohno, Y. Takeda, T. Kondow and H. Sawabe, *J. Phys. Chem. B*, 2001, **105**, 5114–5120.
76 F. Mafuné, J. Kohno, Y. Takeda, T. Kondow and H. Sawabe, *J. Phys. Chem. B*, 2000, **104**, 9111–9117.
77 V. Amendola, S. Polizzi and M. Meneghetti, *J. Phys. Chem. B*, 2006, **110**, 7232–7237.
78 E. Tognoni, V. Palleschi, M. Corsi and G. Cristoforetti, *Spectrochim. Acta, Part B*, 2002, **57**, 1115–1130.
79 S. Heiroth, J. Koch, T. Lippert, A. Wokaun, D. Gunther, F. Garrelie and M. Guillermin, *J. Appl. Phys.*, 2010, **107**, 014908.
80 W. Soliman, N. Takada and K. Sasaki, *Appl. Phys. Express*, 2010, **3**, 5201.
81 Y. Cai and N. Cheung, *Microchem. J.*, 2011, **97**, 109–112.
82 S. Wei and K. Saitow, *Rev. Sci. Instrum.*, 2012, **83**, 073110.
83 L. Lavisse, J. Le Garrec, L. Hallo, J. Jouvard, S. Carles, J. Perez, J. Mitchell, J. Decloux, M. Girault and V. Potin, *Appl. Phys. Lett.*, 2012, **100**, 164103.
84 A. Plech, V. Kotaidis, M. Lorenc and J. Boneberg, *Nat. Phys.*, 2005, **2**, 44–47.
85 A. Plech, V. Kotaidis, S. Grésillon, C. Dahmen and G. von Plessen, *Phys. Rev. B: Condens. Matter Mater. Phys.*, 2004, **70**, 195423.
86 T. Tsuji, K. Iryo, Y. Nishimura and M. Tsuji, *J. Photochem. Photobiol., A*, 2001, **145**, 201–207.
87 Z. Yan, R. Bao, Y. Huang, A. Caruso, S. B. Qadri, C. Z. Dinu and D. B. Chrisey, *J. Phys. Chem. C*, 2010, **114**, 3869–3873.
88 S. Besner, A. V. Kabashin, F. M. Winnik and M. Meunier, *J. Phys. Chem. C*, 2009, **113**, 9526–9531.
89 Z. Lin, E. Leveugle, E. M. Bringa and L. V. Zhigilei, *J. Phys. Chem. C*, 2009, **114**, 5686–5699.
90 J. P. Sylvestre, A. V. Kabashin, E. Sacher and M. Meunier, *Appl. Phys. A: Mater. Sci. Process.*, 2005, **80**, 753–758.
91 K. Niu, J. Yang, S. Kulinich, J. Sun, H. Li and X. Du, *J. Am. Chem. Soc.*, 2010, **132**, 9814–9819.
92 K. Y. Niu, J. Yang, S. A. Kulinich, J. Sun and X. W. Du, *Langmuir*, 2010, **26**, 16652–16657.
93 M. A. Sobhan, M. Ams, M. J. Withford and E. M. Goldys, *J. Nanopart. Res.*, 2010, **12**, 2831–2842.
94 J. Jakobi, S. Petersen, A. Menendez-Manjon, P. Wagener and S. Barcikowski, *Langmuir*, 2010, **26**, 6892–6897.
95 Y. Y. Fong, J. R. Gascooke, B. R. Visser, G. F. Metha and M. A. Buntine, *J. Phys. Chem. C*, 2010, **114**, 15931–15940.
96 J. P. Sylvestre, A. V. Kabashin, E. Sacher, M. Meunier and J. H. Luong, *J. Am. Chem. Soc.*, 2004, **126**, 7176–7177.
97 K. Siskova, B. Vlckova, P. Y. Turpin and C. Fayet, *J. Phys. Chem. C*, 2008, **112**, 4435–4443.
98 C. He, T. Sasaki, Y. Zhou, Y. Shimizu, M. Masuda and N. Koshizaki, *Adv. Funct. Mater.*, 2007, **17**, 3554–3561.
99 Z. Yan, R. Bao and D. B. Chrisey, *Langmuir*, 2011, **27**, 851–855.
100 C. Liang, Y. Shimizu, M. Masuda, T. Sasaki and N. Koshizaki, *Chem. Mater.*, 2004, **16**, 963–965.
101 C. He, T. Sasaki, H. Usui, Y. Shimizu and N. Koshizaki, *J. Photochem. Photobiol., A*, 2007, **191**, 66.
102 E. Jiménez, K. Abderrafi, R. Abargues, J. L. Valdés and J. P. Martínez-Pastor, *Langmuir*, 2010, **26**, 7458–7463.
103 R. Battino, T. R. Rettich and T. Tominaga, *J. Phys. Chem. Ref. Data*, 1983, **12**, 164–177.
104 W. R. Baird and R. T. Foley, *J. Chem. Eng. Data*, 1972, **17**, 355–357.
105 H. Muto, K. Yamada, K. Miyajima and F. Mafuné, *J. Phys. Chem. C*, 2007, **111**, 17221–17226.
106 D. Werner, S. Hashimoto, T. Tomita, S. Matsuo and Y. Makita, *J. Phys. Chem. C*, 2008, **112**, 1321–1329.
107 G. Compagnini, A. Scalisi and O. Puglisi, *J. Appl. Phys.*, 2003, **94**, 7874–7877.
108 G. Compagnini, G. Patané, L. D'Urso, O. Puglisi, R. S. Cataliotti and B. Pignataro, *J. Phys. Chem. C*, 2008, **112**, 20301–20306.
109 L. D'Urso, G. Grasso, E. Messina, C. Bongiorno, V. Scuderi, S. Scalese, O. Puglisi, G. Spoto and G. Compagnini, *J. Phys. Chem. C*, 2009, **114**, 907–915.
110 E. Giorgetti, M. Muniz-Miranda, P. Marsili, D. Scarpellini and F. Giammanco, *J. Nanopart. Res.*, 2012, **14**, 1–13.
111 G. Cristoforetti, E. Pitzalis, R. Spiniello, R. Ishak, F. Giammanco, M. Muniz-Miranda and S. Caporali, *Appl. Surf. Sci.*, 2012, **258**, 3289.
112 P. Boyer and M. Meunier, *J. Phys. Chem. C*, 2012, **116**, 8014–8019.
113 V. Amendola, G. A. Rizzi, S. Polizzi and M. Meneghetti, *J. Phys. Chem. B*, 2005, **109**, 23125–23128.

Published on 01 November 2012. Downloaded by Universidade Federal do Parana on 22/05/2013 04:05:36.

114 G. Compagnini, A. A. Scalisi and O. Puglisi, *Phys. Chem. Chem. Phys.*, 2002, **4**, 2787–2791.
115 K. Saitow, Y. Okamoto and Y. F. Yano, *J. Phys. Chem. C*, 2012, **116**, 17252–17258.
116 K. Saitow, T. Yamamura and T. Minami, *J. Phys. Chem. C*, 2008, **112**, 18340–18349.
117 P. Moroshkin, V. Lebedev, B. Grobéty, C. Neururer, E. Gordon and A. Weis, *Europhys. Lett.*, 2010, **90**, 34002.
118 V. Amendola, S. Polizzi and M. Meneghetti, *Langmuir*, 2007, **23**, 6766–6770.
119 V. Amendola, O. Bakr and F. Stellacci, *Plasmonics*, 2010, **5**, 85–97.
120 A. Schwenke, P. Wagener, S. Nolte and S. Barcikowski, *Appl. Phys. A: Mater. Sci. Process.*, 2011, **104**, 77–82.
121 T. Sugimoto and E. Matijevi, *J. Colloid Interface Sci.*, 1980, **74**, 227–243.
122 H. Yokoi and T. Kantoh, *Bull. Chem. Soc. Jpn.*, 1993, **66**, 1536–1541.
123 R. Sergiienko, E. Shibata, Z. Akase, H. Suwa, T. Nakamura and D. Shindo, *Mater. Chem. Phys.*, 2006, **98**, 34–38.
124 T. Tsuji, T. Hamagami, T. Kawamura, J. Yamaki and M. Tsuji, *Appl. Surf. Sci.*, 2005, **243**, 214–219.
125 H. Y. Kwong, M. H. Wong, C. W. Leung, Y. W. Wong and K. H. Wong, *J. Appl. Phys.*, 2010, **108**, 034304.
126 J. Zhang and C. Q. Lan, *Mater. Lett.*, 2008, **62**, 1521–1524.
127 C. Lin, S. Chen and P. Shen, *J. Phys. Chem. C*, 2009, **113**, 16356–16363.
128 M. Muniz-Miranda, C. Gellini and E. Giorgetti, *J. Phys. Chem. C*, 2011, **115**, 5021–5027.
129 A. Nath and A. Khare, *J. Appl. Phys.*, 2011, **110**, 043111.
130 X. Z. Lin, P. Liu, J. M. Yu and G. W. Yang, *J. Phys. Chem. C*, 2009, **113**, 17543–17547.
131 H. Zhang, C. Liang, Z. Tian, G. Wang and W. Cai, *J. Phys. Chem. C*, 2010, **114**, 12524–12528.
132 J. S. Golightly and A. Castleman Jr, *J. Phys. Chem. B*, 2006, **110**, 19979–19984.
133 T. Sasaki, C. Liang, W. T. Nichols, Y. Shimizu and N. Koshizaki, *Appl. Phys. A: Mater. Sci. Process.*, 2004, **79**, 1489–1492.
134 T. Sasaki, Y. Shimizu and N. Koshizaki, *J. Photochem. Photobiol., A*, 2006, **182**, 335.
135 D. van't Zand, P. Nachev, R. Rosenfeld, P. Wagener, A. Pich, D. Klee and S. Barcikowski, *J. Laser Micro/Nanoeng.*, 2012, **7**, 21–27.
136 Q. Li, C. Liang, Z. Tian, J. Zhang, H. Zhang and W. Cai, *CrystEngComm*, 2012, **14**, 3236–3240.
137 H. Zhang, G. Duan, Y. Li, X. Xu, Z. Dai and W. Cai, *Cryst. Growth Des.*, 2012, **12**, 2646–2652.
138 D. Tan, G. Lin, Y. Liu, Y. Teng, Y. Zhuang, B. Zhu, Q. Zhao and J. Qiu, *J. Nanopart. Res.*, 2011, **13**, 1183–1190.
139 T. X. Phuoc, B. H. Howard, D. V. Martello, Y. Soong and M. K. Chyu, *Optics Lasers Eng.*, 2008, **46**, 829–834.
140 E. Stratakis, M. Barberoglou, C. Fotakis, G. Viau, C. Garcia and G. A. Shafeev, *Opt. Express*, 2009, **17**, 12650–12659.
141 C. C. Huang, C. S. Yeh and C. J. Ho, *J. Phys. Chem. B*, 2004, **108**, 4940–4945.
142 N. Acacia, F. Barreca, E. Barletta, D. Spadaro, G. Currò and F. Neri, *Appl. Surf. Sci.*, 2010, **256**, 6918–6922.
143 P. Liu, C. Wang, J. Chen, N. Xu, G. Yang, N. Ke and J. Xu, *J. Phys. Chem. C*, 2009, **113**, 12154–12161.
144 K. Abderrafi, R. Garcia Calzada, M. B. Gongalsky, I. Suarez, R. Abarques, V. S. Chirvony, V. Y. Timoshenko, R. Ibanez and J. P. Martinez-Pastor, *J. Phys. Chem. C*, 2011, **115**, 5147–5151.
145 P. G. Kuzmin, G. A. Shafeev, V. V. Bukin, S. V. Garnov, C. Farcau, R. Carles, B. Warot-Fontrose, V. Guieu and G. Viau, *J. Phys. Chem. C*, 2010, **114**, 15266–15273.
146 R. Intartaglia, K. Bagga, M. Scotto, A. Diaspro and F. Brandi, *Opt. Mater. Express*, 2012, **2**, 510–518.
147 P. Liu, C. Wang, X. Chen and G. Yang, *J. Phys. Chem. C*, 2008, **112**, 13450–13456.
148 P. Liu, Y. L. Cao, X. Y. Chen and G. W. Yang, *Cryst. Growth Des.*, 2009, **9**, 1390–1393.
149 T. Salminen, J. Dahl, M. Tuominen, P. Laukkanen, E. Arola and T. Niemi, *Opt. Mater. Express*, 2012, **2**, 799–813.
150 K. Anikin, N. Melnik, A. Simakin, G. Shafeev, V. Voronov and A. Vitukhnovsky, *Chem. Phys. Lett.*, 2002, **366**, 357–360.
151 N. Semaltianos, S. Logothetidis, W. Perrie, S. Romani, R. Potter, M. Sharp, P. French, G. Dearden and K. Watkins, *Appl. Phys. A: Mater. Sci. Process.*, 2009, **94**, 641–647.
152 J. Zhang, D. N. Oko, S. Garbarino, R. Imbeault, M. Chaker, A. C. Tavares, D. Guay and D. Ma, *J. Phys. Chem. C*, 2012, **116**, 13413–13420.
153 Y. Ishikawa, K. Kawaguchi, Y. Shimizu, T. Sasaki and N. Koshizaki, *Chem. Phys. Lett.*, 2006, **428**, 426–429.
154 D. Amans, C. Malaterre, M. Diouf, C. Mancini, F. Chaput, G. Ledoux, G. Breton, Y. Guillin, C. Dujardin and K. Masenelli-Varlot, *J. Phys. Chem. C*, 2011, **115**, 5131–5139.
155 G. Ledoux, D. Amans, C. Dujardin and K. Masenelli-Varlot, *Nanotechnology*, 2009, **20**, 445605.
156 S. W. Mhin, J. H. Ryu, K. M. Kim, G. S. Park, H. W. Ryu, K. B. Shim, T. Sasaki and N. Koshizaki, *Nanoscale Res. Lett.*, 2009, **4**, 888–895.
157 M. Ishizaki, T. Katagiri, T. Sasagawa, Y. Kitamoto, O. Odawara and H. Wada, *J. Nanotechnol.*, 2012, **2012**.
158 Y. Liang, P. Liu, H. Li and G. Yang, *CrystEngComm*, 2012, **14**, 3291–3296.
159 G. Lin, D. Tan, F. Luo, D. Chen, Q. Zhao, J. Qiu and Z. Xu, *J. Alloys Compd.*, 2010, **507**, L43–L46.
160 S. W. Mhin, J. H. Ryu, K. M. Kim, G. S. Park, H. W. Ryu, K. B. Shim, T. Sasaki and N. Koshizaki, *Appl. Phys. A: Mater. Sci. Process.*, 2009, **96**, 435–440.
161 M. Nath, C. Rao, R. Popovitz-Biro, A. Albu-Yaron and R. Tenne, *Chem. Mater.*, 2004, **16**, 2238–2243.
162 L. Nistor, G. Epurescu, M. Dinescu and G. Dinescu, *IOP Conf. Ser.: Mater. Sci. Eng.*, 2010, **15**, 012067.
163 Q. Liu, C. Wang and G. Yang, *Phys. Rev. B: Condens. Matter Mater. Phys.*, 2005, **71**, 155422.
164 A. Menéndez-Manjón, B. N. Chichkov and S. Barcikowski, *J. Phys. Chem. C*, 2010, **114**, 2499–2504.
165 K. Saitow, *J. Phys. Chem. B*, 2005, **109**, 3731–3733.
166 K. Sasaki, T. Nakano, W. Soliman and N. Takada, *Appl. Phys. Express*, 2009, **2**, 046501.

 This journal is © the Owner Societies 2013